Two-exciton spectroscopy of photosynthetic antenna complexes: Collective oscillator analysis

O. Kühn, V. Chernyak, and S. Mukamel
Department of Chemistry, University of Rochester, Rochester, New York 14627

(Received 14 May 1996; accepted 9 August 1996)

The linear and third-order polarizabilities of the light-harvesting antennae of photosynthetic bacteria and green plants are calculated using an equation of motion approach which maps the system onto a coupled set of anharmonic excitonic oscillators. The oscillator representation is shown to have several advantages over the traditional picture based on properties of individual global eigenstates of the aggregate; besides a considerable reduction of computational effort, the dynamics of excitations in the two-exciton band is conveniently analyzed in terms of single-exciton Green's functions and the two-exciton scattering matrix. © *1996 American Institute of Physics.* [S0021-9606(96)04142-6]

I. INTRODUCTION

The primary processes of photosynthesis, the capture of sun light, and the subsequent conversion into chemical energy, constitute the very basis of all life. The high efficiency and flexibility of theses processes, which take place in green plants, photosynthetic bacteria, and certain algae, make them an intriguing subject to study.[1] Recently, high resolution structural data of various photosynthetic antenna complexes became available.[2–4] The possibility to unravel the relationship between microscopic structure and optical response triggered a host of spectroscopic investigations.

One of the most extensively studied systems is the antenna complex of purple bacteria. In many cases one can distinguish between a core antenna (LH1) surrounding the reaction center and an outer antenna (LH2), both having a circular symmetry. To date, high resolution (2.5 Å) data, which allow for a clear assignment of protein and pigment molecules, are available for the LH2 of *Rhodopseudomonas (Rps.) acidophila*[3] only. Using these data and a fit of the linear absorption and circular dichroism lineshapes, K. Sauer and coworkers[5] recently proposed interaction energies between pigments as well as molecular transition energies. The LH2 exhibits two distinct absorption maxima in the spectral region between 800 and 900 nm. In the wild-type *Rhodobacter (Rb.) sphaeroides*, for instance, these are located at about 800 nm (B800) and 850 nm (B850). The position of the B850 band, however, can be experimentally varied by means of site-directed mutagenesis.[6] The structure of LH1 is known only to a 8.5 Å resolution, indicating the overall symmetry of the complex.[4] The relevant absorption maximum of this core antenna is typically at about 875 nm (B875).

Various ultrafast spectroscopic techniques, such as one- and two-color pump-probe,[7] time-integrated two- and three-pulse photon echo,[8] and transient grating[8] have been employed in order to determine the relevant time scales for exciton motion in the antenna complex, which range from about 0.7 ps (B800→ B850) to 2.6 ps (B850 → B875) at room temperature. The role of the spectral overlap between the B800 and the B850 bands for the excitation energy transfer has been highlighted in a subpicosecond one-color pump-probe study of site-directed mutants of the LH2 of *Rb. sphaeroides* at 77 K.[9] It was found that with increasing blue shift of the B850 band relative to the unchanged B800 band the transfer becomes faster, as predicted by Förster's theory.

The structure of green plants antenna complexes lacks the high symmetry found in LH1 and LH2. Electron diffraction on two-dimensional crystals of the Chl a/b containing complex related to photosystem II (LHC-II) revealed twelve chlorophyll molecules (7 Chl a, 5 Chl b) arranged in two layers within the thylakoid membrane.[2] In contrast to the bacterial antennae the current resolution of 3.4 Å does not allow the determination of orientations of the transition dipoles in the membrane. Hence the simulation of the linear absorption spectrum of LHC-II becomes more involved as will be shown below. The low temperature spectrum shows three major peaks at about 650 nm (Chl b), 671 nm (Chl a), and 676 nm (Chl a). The time scales found for energy transfer between the Chl b and Chl a pigment pools using the pump-probe technique range from 500 fs[10] to 150 fs.[11] Transfer times of 500 fs[12] and 250 fs[13] have been derived from ultrafast fluorescence measurements. Very recently a comprehensive study of the energy transfer covering a broad spectral range clearly demonstrated a multitude of time scales from several hundred femtoseconds to some tens of picoseconds.[14]

With the advent of ultrafast nonlinear optical spectroscopies the dynamics of excitons in molecular aggregates has attracted considerable attention. Phenomena arising upon aggregation, such as exciton cooperativity and two-exciton resonances, have been discussed in great detail for dye-aggregates (e.g., the J-aggregate pseudoisocyanine[15]) and very recently for photosynthetic antenna systems.[1] Aggregates made of multi-level molecules show two types of two-exciton states. The first originates from intramolecular transitions and exists also in the monomer. We shall denote these molecular double excitations (MDE). The second type are delocalized excited states whose oscillator strength is induced by the intermolecular dipole–dipole interaction, which can become rather strong for the observed distances between certain pigments of about 8–10 Å. They will be denoted

Downloaded¬08¬Mar¬2001¬to¬128.151.176.185.¬Redistribution¬subject¬to¬AIP¬copyright,¬see¬http://ojps.aip.org/jcpo/jcpcpyrts.html

collective double excitations (CDE). Depending on the aggregate geometry and energetics MDE and CDE can be strongly mixed. We shall refer to the entire two-exciton manifold in the aggregate, representing the coupled MDE and CDE, as the two-exciton band.

The importance of the incorporation of MDE of the BChl *a* monomers in the interpretation of pump-probe data obtained for *Rb. sphaeroides* was recently emphasized by Sundström and coworkers.[16] The possibility of singlet excited state absorption has also been discussed for the LHC-II system.[11,14,17] The interplay between MDE and CDE was recently studied for linear aggregates.[18]

From the theoretical point of view, the description of the nonlinear optical response by means of equations of motion for a set of relevant exciton variables has proven to be advantageous compared with, for instance, a sum-over-states (SOS) approach, which is based on a complete knowledge of the global eigenstates of the system. An intuitive picture emerges in which the aggregate is viewed as a collection of coupled driven anharmonic oscillators.[19] This approach further results in a considerable reduction of the numerical effort. It becomes particularly attractive when only a few oscillators dominate the optical response. This enables us to investigate larger aggregates such as the photosynthetic antenna complexes.

In this paper we apply the excitonic oscillator Green's function approach to the analysis of two-exciton dynamics and their spectroscopic signatures in pigment-protein complexes of photosynthetic antennae. Our primary goal is to highlight the relation between antenna geometry and energetics and its two-photon spectroscopy using a rigorous theoretical model. In Appendix A we show how the Hamiltonian representing an aggregate of multi-level molecules can be recast in terms of coupled anharmonic oscillators. In Section II we use this representation to calculate the first- and the third-order polarizabilities of aggregates made of three-level molecules having an arbitrary geometry. The optical susceptibilities are given in terms of single-exciton Green's functions and the exciton–exciton scattering matrix. We further compare the excitonic oscillator picture with the standard sum-over-states (SOS) approach which is based on the global aggregate electronic eigenstates. Numerical results for the two-photon absorption spectrum are presented in Section III. We first study a dimer to illustrate how different resonances show up in the Green's function expression (GFE). We next apply our model to the LH2 and LHC-II antenna complexes and analyze the two-exciton spectroscopic features. The results are summarized in Section IV.

II. EXCITONIC–OSCILLATOR PICTURE FOR COUPLED MULTI–LEVEL MOLECULES

We consider an aggregate made of N molecules each described by three electronic states S_0, S_1, and S_2[24]. We assume that only the $S_0 \rightarrow S_1$ and the $S_1 \rightarrow S_2$ transitions have finite matrix elements of the transition dipole moment denoted by $\mu_n^{(10)}$ and $\mu_n^{(21)}$. The molecules interact via dipole–dipole interaction. The Hamiltonian will be first expressed in terms of exciton creation and annihilation operators, $b_{nf}^\dagger$ and b_{nf}, which obey the Pauli-commutation relations,[21]

$$[b_{nf}, b_{n'f'}^\dagger] = \delta_{nn'}\delta_{ff'}(1 - 2b_{nf}^\dagger b_{nf}), \tag{2.1}$$

and are defined by their action on the ground state $|0_n)$, as $b_{nf}^\dagger|0_n) = |f_n)$. Here $f=(1,2)$ denotes the excited states of the n-th molecule ($n=1...N$). The electronic transition energies (with respect to the ground state) are $\hbar\Omega_n^{(f)}$. Exciton dynamics in molecular aggregates is generally subject to various relaxation and dephasing processes. We will neglect pure dephasing and consider a finite excited state lifetime as the only source of line broadening at this point. The inverse lifetimes of the S_1 and S_2 states will be denoted as $\gamma_n^{(1)}$ and $\gamma_n^{(2)}$, respectively. Transition frequencies and inverse lifetimes will be combined in the complex frequencies, $\tilde{\Omega}_n^{(f)} = \Omega_n^{(f)} - i\gamma_n^{(f)}$.

The Frenkel Hamiltonian is given by

$$H' = H_0' + H_{\mathrm{d-d}}', \tag{2.2}$$

with the monomer contribution

$$H_0' = \sum_{n,f=(1,2)} \hbar\tilde{\Omega}_n^{(f)} b_{nf}^\dagger b_{nf}, \tag{2.3}$$

and $H_{\mathrm{d-d}}'$ is the intermolecular dipole–dipole interaction. We assume that both transition dipoles of each molecule are parallel and oriented along the unit vector $\hat{\mu}_n$. The molecular dipole operator then has the form $\vec{d}_n = \hat{\mu}_n d_n$, and the intermolecular dipole–dipole interaction operator reads[21]

$$H_{\mathrm{d-d}}' = \sum_{mn} \beta_{mn} d_m d_n, \tag{2.4}$$

with the dipole operator

$$d_n = \mu_n^{(10)}(b_{n1}^\dagger + b_{n1}) + \mu_n^{(21)}(b_{n2}^\dagger b_{n1} + b_{n1}^\dagger b_{n2}), \tag{2.5}$$

and the orientational factor given by

$$\beta_{mn} = [\hat{\mu}_m \cdot \hat{\mu}_n - 3\hat{r}_{mn} \cdot \hat{\mu}_m \hat{r}_{mn} \cdot \hat{\mu}_n]/r_{mn}^3. \tag{2.6}$$

Here $r_{mn} = |\vec{r}_m - \vec{r}_n|$ is the distance between the m-th and the n-th molecule, and $\hat{r}_{mn}$ is the corresponding unit vector.

Below we present the coupled oscillator representation for the nonlinear optical response of this aggregate. This is a direct extension of our previous calculations for two-level molecules[22] to include a third intramolecular level (i.e., MDE). The level scheme of each molecule can be represented using an excitonic oscillator as shown in Appendix A. To that end we introduce creation (annihilation) operators, $B_n^\dagger$ (B_n), which generate the oscillator states and satisfy the following commutation relations [see Eq. (A7)]:

$$[B_m, B_n^\dagger] = \delta_{mn}(1 - (2 - \kappa_m^2) B_m^\dagger B_m). \tag{2.7}$$

Here we introduced the parameter κ_m representing the ratio between the transition dipole moments for $S_1 \rightarrow S_2$ and $S_0 \rightarrow S_1$ transitions (see Table I). Excited molecular states are obtained by successive application of $B_n^\dagger$ to the vacuum state $|0_n\rangle$. Using Eq. (2.7) one has for the normalized molecular states

Downloaded¬08¬Mar¬2001¬to¬128.151.176.185.¬Redistribution¬subject¬to¬AIP¬copyright,¬see¬http://ojps.aip.org/jcpo/jcpcpyrts.html

TABLE I. Correspondence between the parameters of the Frenkel Hamiltonian [Eqs. (2.3) and (2.4)] and the oscillator Hamiltonian [Eqs. (2.9) and (2.10)]. Λ_n is chosen to reproduce the lifetimes for the S_2 states.

	Oscillator Hamiltonian	Frenkel Hamiltonian
Oscillator frequency	$\hbar\Omega_n$	$\hbar\Omega_n^{(1)}$
Nonlinearity	g_n	$2\hbar(\Omega_n^{(2)}\kappa_n^{-2}-\Omega_n^{(1)})$
Inverse lifetime S_1	Γ_n	$\gamma_n^{(1)}$
	Λ_n	$-2(\gamma_n^{(2)}\kappa_n^{-2}-\Gamma_n)$
Transition dipole $S_0 \rightarrow S_1$	μ_n	$\mu_n^{(10)}$
Ratio transition dipoles	κ_n	$\mu_n^{(21)}/\mu_n^{(10)}$
Hopping matrix (S_1)	J_{mn}	$\beta_{mn}\mu_m^{(10)}\mu_n^{(10)}$

$$|0_n\rangle, \quad |1_n\rangle = B_n^\dagger|0_n\rangle, \quad |2_n\rangle = \kappa_n^{-1}(B_n^\dagger)^2|0_n\rangle,$$

where $|1_n\rangle$ and $|2_n\rangle$ represent the states S_1 and S_2 of the nth molecule.

Using these variables the Hamiltonian is now written in the form

$$H = H_0 + H_{\mathrm{d-d}}, \tag{2.8}$$

with

$$H_0 = \sum_n \left[\hbar\tilde{\Omega}_n B_n^\dagger B_n + \frac{\tilde{g}_n}{2}(B_n^\dagger)^2(B_n)^2\right], \tag{2.9}$$

and

$$H_{\mathrm{d-d}} = \sum_{mn} [J_{mn}B_m^\dagger B_n + \mathrm{c.c.}]. \tag{2.10}$$

Here $\tilde{\Omega}_n = \Omega_n - i\Gamma_n$, $\tilde{g}_n = g_n + i\hbar\Lambda_n$, J_{mn} is the hopping matrix, and the molecular dipole operator is taken to be linear in the new operators,

$$\vec{d}_n = \vec{\mu}_n(B_n^\dagger + B_n). \tag{2.11}$$

The new parameters $\tilde{\Omega}_n$, μ_n, and $\tilde{g}_n$ as well as the ratio κ_n may be expressed in terms of the transition energies and the transition dipole matrix elements, which characterize the system according to Eqs. (2.3) and (2.5) for a given geometry. This is done by comparing the relevant matrix elements of H_0 and H_0' as well as the molecular dipole operators. All the parameters of Eqs. (2.9) and (2.10) are uniquely defined by the parameters of the original Hamiltonian (2.2) and are listed in Table I and illustrated in Fig. 1. In Fig. 1 we also

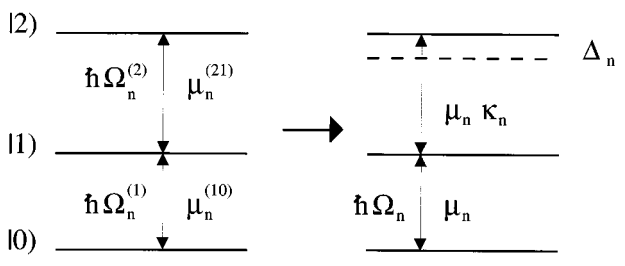

FIG. 1. Mapping of the three-level Frenkel model (left) onto the excitonic oscillator model (right).

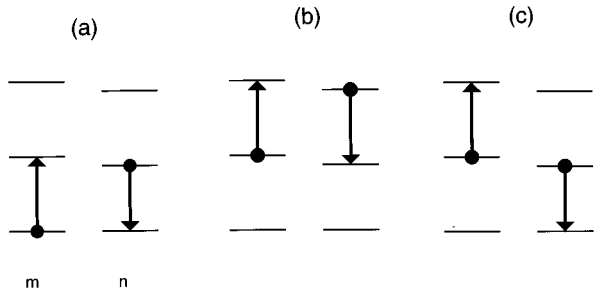

FIG. 2. Possible resonant energy transfer processes in a dimer made of three-level molecules.

introduce the quantity $\Delta_n = \hbar\Omega_n^{(2)} - 2\hbar\Omega_n^{(1)}$ to denote the anharmonicity of each oscillator. Using the oscillator Hamiltonian parameters we have $\Delta_n = \kappa_n^2 g_n/2 + (\kappa_n^2 - 2)\hbar\Omega_n$.

We note the following two limits of our excitonic oscillator model. For $\kappa_n = 0$, the $S_1 \rightarrow S_2$ transition is forbidden and we recover the model aggregate of two-level molecules.[19] When $\kappa_n = \sqrt{2}$ and $\Delta_n = 0$, the system is harmonic and the third-order nonlinear optical response vanishes identically. This results from interference between ''two-level'' contributions involving states S_0 and S_1 alone and ''three-level'' contributions which also include S_2.[19] The two sources of nonlinearities in the present model are therefore the anharmonicity Δ_n and the deviation of κ_n from the harmonic oscillator value $\sqrt{2}$. In molecular crystals and aggregates such as the antenna complexes, the transition energies are large compared with the intermolecular coupling. We further assume that Δ_n is small compared to the electronic transition energies. Thus only the resonant processes shown in Fig. 2 give significant contributions to $H_{\mathrm{d-d}}$. We have energy transfer involving the S_1-state [Fig. 2(a)]. The presence of higher excited states leads to energy transfer involving the S_1- and S_2-states [Fig. 2(b)]. The process shown in Fig. 2c can result in exciton–exciton annihilation provided it is followed by a fast internal conversion of S_2 to S_1.

III. EQUATIONS OF MOTION AND GREEN'S FUNCTION EXPRESSIONS FOR THE OPTICAL RESPONSE

To calculate the nonlinear optical polarizabilities of our system we need to introduce its coupling with the radiation field. The total Hamiltonian becomes

$$H_{\mathrm{tot}}(t) = H + H_{\mathrm{F}}(t), \tag{3.1}$$

where the aggregate Hamiltonian, H, is given in Eq. (2.8), and the coupling to the classical external field $\vec{E}(\vec{r},t)$ is

$$H_{\mathrm{F}}(t) = -\sum_n \vec{d}_n\vec{E}(\vec{r}_n,t). \tag{3.2}$$

We will calculate the response to third order in the external field using the equation of motion approach.[22] In general the dynamics of one-exciton variables $\langle B_n\rangle$ is coupled to the higher-order exciton variables $\langle B_m^\dagger B_n\rangle$ and $\langle B_m^\dagger B_n B_p\rangle$. It was shown in Ref. 19 that in the absence of pure dephasing one can invoke the factorizations $\langle B_m^\dagger B_n\rangle = \langle B_m^\dagger\rangle\langle B_n\rangle$ and $\langle B_m^\dagger B_n B_p\rangle = \langle B_m^\dagger\rangle\langle B_n B_p\rangle$. Apart from additional contribu-

Downloaded¬08¬Mar¬2001¬to¬128.151.176.185.¬Redistribution¬subject¬to¬AIP¬copyright,¬see¬http://ojps.aip.org/jcpo/jcpcpyrts.html

tions to the line broadening, pure dephasing also requires extending the equations of motion to include additional dynamical variables.[15,19,23] In general pure dephasing due to the coupling between exciton dynamics and phonon modes of the environment cannot be neglected in photosynthetic antenna complexes. In order to investigate the principal spectroscopic signatures of the two-exciton band in structurally different aggregates, however, we will neglect such processes in the following discussion. This is justified, for instance, at low temperatures, where the fluctuations of the environment are approximately frozen in. Hence we need to consider only the evolution of the two-exciton variable $\langle B_m B_n\rangle$ in addition to the single exciton variables $\langle B_n\rangle$. The resulting equations of motion are

$$i\hbar\frac{d}{dt}\langle B_m\rangle-\sum_n h_{mn}\langle B_n\rangle = \langle B_m^\dagger\rangle\sum_{nkl}[\mathscr{U}_{mn,kl}\langle B_k B_l\rangle + \mathscr{P}_{mn,kl}[\langle B_k\rangle E_l(t)+E_k(t)\langle B_l\rangle]], \tag{3.3}$$

and

$$i\hbar\frac{d}{dt}\langle B_n B_m\rangle-\sum_{kl}(\mathscr{T}_{mn,kl}+\mathscr{U}_{mn,kl})\langle B_k B_l\rangle = -\sum_{kl}(\delta_{mk}\delta_{nl}-\mathscr{P}_{mn,kl})(\langle B_k\rangle E_l(t)+E_k(t))\langle B_l\rangle). \tag{3.4}$$

Here we defined the matrices

$$h_{mn}=\delta_{mn}\hbar\tilde{\Omega}_m+J_{mn}, \tag{3.5}$$

$$\mathscr{T}_{mn,kl}=h_{mk}\delta_{nl}+\delta_{mk}h_{nl}, \tag{3.6}$$

$$\mathscr{U}_{mn,kl}=\delta_{mn}\frac{1}{2}[\delta_{mk}\delta_{nl}\kappa_m^2\tilde{g}_m+(\kappa_m^2-2)\mathscr{T}_{mn,kl}], \tag{3.7}$$

and

$$\mathscr{P}_{mn,kl}=\delta_{mn}\delta_{mk}\delta_{nl}\left(1-\frac{\kappa_m^2}{2}\right). \tag{3.8}$$

We have introduced the notation $E_n(t)=\vec{\mu}_n\vec{E}(\vec{r}_n,t)$. Note that the resonant energy transfer between S_1 and S_2 (Fig. 1b) does not contribute to the third-order signal.

Assuming that the aggregate is small compared with the optical wavelength, its optical response is determined by the expectation value of the polarization operator $P=\Sigma_n\mu_n(B_n^\dagger+B_n)$. The optical susceptibilities are then defined by

$$P(\omega)=\chi^{(1)}(-\omega;\omega)\mathscr{E}_1+\chi^{(2)}(-\omega_s;\omega_1,\omega_2)\mathscr{E}_1\mathscr{E}_2+\chi^{(3)}(-\omega_s;\omega_1,\omega_2,\omega_3)\mathscr{E}_1\mathscr{E}_2\mathscr{E}_3+\cdots. \tag{3.9}$$

Here, $\mathscr{E}_j$ is the amplitude of the j-th mode of the field with frequency ω_j.

The formal structure of Eqs. (3.3) and (3.4) has been investigated previously.[36] Following Ref. 36 we express the optical response in terms of the one-exciton Green's function,

$$G_{mn}(\omega)=[\hbar\omega-h]^{-1}_{mn}. \tag{3.10}$$

The linear susceptibility then reads as

$$\chi^{(1)}(-\omega_1;\omega_1)=-\sum_{m_s m_1}\mu_{m_s}\mu_{m_1}[G_{m_s m_1}(\omega_1)+G^*_{m_s m_1}(-\omega_1)], \tag{3.11}$$

and for the third-order susceptibility we obtain

$$\chi^{(3)}(-\omega_s;\omega_1,\omega_2,\omega_3) = -\frac{1}{6}\sum_{\text{perm}}\sum_{m_s m_1 m_2 m_3}\mu_{m_s}\mu_{m_1}\mu_{m_2}\mu_{m_3} \times\sum_{mn}G_{m_s m}(\omega_s)G^*_{m m_2}(-\omega_2)\overline{\Gamma}_{mn}(\omega_1+\omega_3) \times G_{n m_1}(\omega_1)G_{n m_3}(\omega_3)+\text{c}'.\text{c}'. \tag{3.12}$$

Here $\omega_s=\omega_1+\omega_2+\omega_3$ and c′.c′. stands for complex conjugation and changing of the signs of all frequencies $\omega_j\rightarrow-\omega_j$ $(j=1,2,3)$. perm denotes the sum over all permutations of pairs (m_j,ω_j). All information about MDE and CDE is included in the scattering matrix $\overline{\Gamma}(\omega)$. Due to the local nature of the commutation relations (2.7), this matrix is not a tetradic $N^2\times N^2$ but a $N\times N$ matrix,

$$\overline{\Gamma}_{mn}(\omega)=[F(\omega)]^{-1}_{mn}[(\hbar\omega+\tilde{g}_n)\kappa_n^2-2\hbar\omega], \tag{3.13}$$

with

$$F_{mn}(\omega)=\delta_{mn}\kappa_m^2-[(\hbar\omega+\tilde{g}_m)\kappa_m^2-2\hbar\omega]\mathscr{G}_{mn}(\omega), \tag{3.14}$$

and the zero-order two-exciton Green's function is given by[19]

$$\mathscr{G}_{mn}(\omega)=\int\frac{d\omega'}{2\pi i}G_{mn}(\omega')G_{mn}(\omega-\omega'). \tag{3.15}$$

An important limit of Eq. (3.12) is the local field approximation (LFA). In the equations of motion language the LFA implies a factorization of the intermolecular two-exciton variables $\langle B_m B_n\rangle=\langle B_m\rangle\langle B_n\rangle(1-\delta_{nm})+\langle B_m B_m\rangle\delta_{nm}$. Inserting this into Eqs. (3.3) and (3.4) yields the following approximation for the scattering matrix:

$$\overline{\Gamma}^{\text{LFA}}_{mn}(\omega)=\delta_{mn}\frac{\hbar}{2}(\omega-2\Omega_m)\times\left[\frac{\kappa_m^2}{\hbar}\frac{\Delta_m}{\omega-(2\Omega_m+\Delta_m/\hbar)+i\gamma_m^{(2)}}+(\kappa_m^2-2)\right]. \tag{3.16}$$

The structure of the two-exciton scattering matrix [Eq. (3.13) or (3.16)] reflects the roles of statistics and anharmonicities in the optical nonlinearities. Obviously, $\overline{\Gamma}(\omega)$ reduces to the

Downloaded¬08¬Mar¬2001¬to¬128.151.176.185.¬Redistribution¬subject¬to¬AIP¬copyright,¬see¬http://ojps.aip.org/jcpo/jcpcpyrts.html

two-level limit with Pauli statistics ($\kappa_n=0$)[22] as well as to the limit of three-level anharmonic oscillators with Bose statistics ($\kappa_n=\sqrt{2}$, anharmonicity $\Delta_n=g_n$). The latter case has been used to treat excitons in coupled two-level systems as soft-core bosons.[23] Double occupation of an excited state is discouraged by means of a repulsive potential in the Hamiltonian Eq. (2.9), with strength g_n. In the limit $g_n\to\infty$, the exciton scattering matrix for Paulions (hard-core bosons) is recovered.[19]

The advantages of the excitonic oscillator compared with the SOS-approach have been demonstrated earlier.[19] For aggregates consisting of coupled three-level molecules the SOS-method requires the calculation of $2N+(N-1)N/2$ eigenstates, i.e. N more than in the two-level case. On the other hand, in the GFE the third level merely leads to a modification of the scattering matrix retaining its $N\times N$ dimensionality.

In order to analyze the numerical results obtained from Eq. (3.12) in the following section it is instructive to introduce the one-exciton eigenstates $|\alpha\rangle$ which satisfy

$$\left[\sum_n \hbar\Omega_n \hat{B}_n^\dagger \hat{B}_n + \sum_{mn} J_{mn}(\hat{B}_m^\dagger \hat{B}_n + \text{c.c.})\right]|\alpha\rangle = \hbar\omega_\alpha|\alpha\rangle, \tag{3.17}$$

with $\hat{B}_n^\dagger(\hat{B}_n)$ obeying Bose statistics ($\kappa_n=\sqrt{2}$). The one-exciton Green's function then becomes

$$G_{mn}(\omega)=\sum_\alpha \langle m|\alpha\rangle\langle\alpha|n\rangle G_\alpha(\omega), \tag{3.18}$$

with

$$G_\alpha(\omega)=\frac{1}{\hbar(\omega-\omega_\alpha+i\Gamma_\alpha)}, \tag{3.19}$$

and for the two-exciton Green's function we have[19]

$$\mathscr{G}_{mn}(\omega)=\frac{1}{\hbar}\sum_{\alpha\beta}\frac{\langle m|\alpha\rangle\langle m|\beta\rangle\langle\beta|n\rangle\langle\alpha|n\rangle}{\omega-\omega_\alpha-\omega_\beta+i(\Gamma_\alpha+\Gamma_\beta)}. \tag{3.20}$$

Here we introduced phenomenological lifetimes (Γ_α^{-1}) for the single-exciton states.[24] Equation (3.12) can then be rewritten as

$$\begin{aligned}\chi^{(3)}(-\omega_s;\omega_1,\omega_2,\omega_3)=&-\frac{1}{6}\sum_{\text{perm}}\sum_{\alpha_1\alpha_2\alpha_3\alpha_4}\mu_{\alpha_1}\mu_{\alpha_2}\mu^*_{\alpha_3}\mu^*_{\alpha_4}\\&\times G_{\alpha_1}(\omega_s)G^*_{\alpha_2}(-\omega_2)G_{\alpha_3}(\omega_1)\\&\times G_{\alpha_4}(\omega_3)\overline{\Gamma}_{\alpha_1\alpha_2,\alpha_3\alpha_4}(\omega_1+\omega_3)\\&+\text{c.}'\text{c.}',\end{aligned} \tag{3.21}$$

where

$$\begin{aligned}\overline{\Gamma}_{\alpha_1\alpha_2,\alpha_3\alpha_4}(\omega)=&\sum_{mn}\langle\alpha_1|m\rangle\langle\alpha_2|m\rangle\\&\times\overline{\Gamma}_{mn}(\omega)\langle n|\alpha_3\rangle\langle n|\alpha_4\rangle,\end{aligned} \tag{3.22}$$

with $\overline{\Gamma}_{mn}(\omega)$ given by Eq. (3.13). The oscillator transition dipole matrix elements are given using the one-exciton eigenstates,

$$\mu_\alpha=\sum_m \mu_m\langle m|\alpha\rangle. \tag{3.23}$$

Equation (3.21) provides a convenient way to trace the origin of different resonances, i.e. the Green's functions and $\overline{\Gamma}(\omega)$, which interfere to give $\chi^{(3)}$. For comparison we give the third-order susceptibility using the SOS-representation,[19]

$$\begin{aligned}&\chi^{(3)}_{\text{SOS}}(-\omega_s;\omega_1,\omega_2,\omega_3)\\&=\frac{1}{6}\sum_{\text{perm}}\sum_{ee'}|\mu_{ge}|^2|\mu_{ge'}|^2 I_{eg}(\omega_s)I^*_{e'g}(-\omega_2)[I_{eg}(\omega_3)\\&\quad+I_{e'g}(\omega_1)]-\frac{1}{6}\sum_{\text{perm}}\sum_{ee'f}\mu_{ge}\mu_{ef}\mu_{fe'}\mu_{e'g}\\&\quad\times I_{fg}(\omega_1+\omega_3)I_{e'g}(\omega_1)[I^*_{eg}(-\omega_2)+I_{eg}(\omega_s)]+\text{c.}'\text{c.}'\end{aligned} \tag{3.24}$$

Here, g denotes the ground state ($\hbar\omega_g=0,\Gamma_g=0$), (e,e') the one-exciton states, f the two-exciton states, μ_{ab} is the matrix element of the transition dipole between states a and b, and

$$I_{ag}(\omega)=\frac{1}{\hbar(\omega-\omega_a+i\Gamma_a)}. \tag{3.25}$$

We shall compare the SOS-expression and the GFE by looking at two-photon absorption and invoking the rotating wave approximation. The SOS-expression gives

$$\begin{aligned}&\chi^{(3)}_{\text{SOS}}(-\omega_2;\omega_1,-\omega_1,\omega_2)\\&=\frac{1}{6}\sum_{ee'}|\mu_{ge}|^2|\mu_{ge'}|^2[I_{eg}(\omega_1)+I_{eg}(\omega_2)]\\&\quad\times[I^*_{e'g}(\omega_1)I_{eg}(\omega_2)+I^*_{eg}(\omega_1)I_{e'g}(\omega_2)]\\&\quad-\frac{1}{6}\sum_{ee'f}\mu_{ge'}\mu_{e'f}\mu_{fe}\mu_{eg}I_{fg}(\omega_1+\omega_2)\\&\quad\times[I_{eg}(\omega_1)+I_{eg}(\omega_2)][I^*_{e'g}(\omega_1)+I_{e'g}(\omega_2)],\end{aligned} \tag{3.26}$$

whereas Eq. (3.21) gives

$$\begin{aligned}&\chi^{(3)}(-\omega_2;\omega_1,-\omega_1,\omega_2)\\&=-\frac{1}{3\hbar^4}\sum_{\alpha_1\alpha_2\alpha_3\alpha_4}\frac{\mu_{\alpha_1}}{\omega_2-\omega_{\alpha_1}+i\Gamma_{\alpha_1}}\\&\quad\times\frac{\mu_{\alpha_2}}{\omega_1-\omega_{\alpha_2}-i\Gamma_{\alpha_2}}\frac{\mu_{\alpha_3}}{\omega_1-\omega_{\alpha_3}+i\Gamma_{\alpha_3}}\\&\quad\times\frac{\mu_{\alpha_4}}{\omega_2-\omega_{\alpha_4}+i\Gamma_{\alpha_4}}\overline{\Gamma}_{\alpha_1\alpha_2,\alpha_3\alpha_4}(\omega_1+\omega_2).\end{aligned} \tag{3.27}$$

The matrix elements $F_{mn}(\omega)$ which enter the scattering matrix can be written as

Downloaded¬08¬Mar¬2001¬to¬128.151.176.185.¬Redistribution¬subject¬to¬AIP¬copyright,¬see¬http://ojps.aip.org/jcpo/jcpcpyrts.html

$$F_{mn}(\omega)=\sum_{\alpha\beta}\frac{\kappa_m^2}{\omega-\omega_\alpha-\omega_\beta+i(\Gamma_\alpha+\Gamma_\beta)}[\delta_{mn}(\omega-\omega_\alpha-\omega_\beta+i(\Gamma_\alpha+\Gamma_\beta))-[\tilde{g}_m/\hbar+(1-2/\kappa_m^2)\omega]\langle m|\alpha\rangle\langle m|\beta\rangle\langle\beta|n\rangle\langle\alpha|n\rangle]. \tag{3.28}$$

In the two-level limit ($\kappa_n=0$) $F_{mn}(\omega)=2\hbar\omega\mathscr{G}_{mn}(\omega)$ contains the interaction-induced two-exciton resonances (CDE) only. For $\kappa_n\neq 0$ the latter are modified, and new resonances show up due to their coupling to the intramolecular S_2 states.

Equation (3.27) will be used in the following Section for the calculation of the third-order response of different aggregates in the frequency-domain. The time-domain response can be calculated by solving the equations of motion (3.3) and (3.4) using numerical integration. Different techniques are characterized by a different wavevector of the signal. The appropriate expressions which allow for a bookkeeping of the wavevector dependence of the excitonic variables are given in Appendix B.

IV. NUMERICAL SIMULATIONS

A. Molecular dimer

Many of the features of two-photon spectroscopy of aggregates can be understood by considering a dimer. We shall therefore start our discussion with a detailed analysis of a dimer made of three-level systems. The one-exciton energies are given by

$$\hbar\omega_\pm=\frac{1}{2}(\hbar(\Omega_1+\Omega_2)\pm\sqrt{\hbar^2(\Omega_1-\Omega_2)^2+4J_{12}^2}), \tag{4.1}$$

with the eigenstates

$$|\alpha=\pm\rangle=\sin\Theta_\pm|1_1\rangle+\cos\Theta_\pm|1_2\rangle, \tag{4.2}$$

and the transformation angles

$$\Theta_\pm=\arctan\left[\frac{1}{2J_{12}}(\hbar(\Omega_2-\Omega_1)\pm\sqrt{\hbar^2(\Omega_2-\Omega_1)^2+4J_{12}^2})\right]. \tag{4.3}$$

Hence we can express Eqs. (3.21)–(3.23) in terms of $\omega_\pm$ and $\Theta_\pm$. In Appendix C we give the scattering matrix $\bar{\Gamma}(\omega)$.

We calculated the differential pump-probe spectrum

$$W_{\mathrm{TPA}}=\mathrm{Im}\,\chi^{(3)}(-\omega_2;\omega_1,-\omega_1,\omega_2). \tag{4.4}$$

In the following we refer to W_{TPA} as the two-photon absorption (TPA) signal. We consider a nondegenerate dimer with $\hbar\Omega_1=1.475$ eV, $\hbar\Omega_2=1.525$ eV, $J_{12}=-0.05$ eV, and $\hbar\Gamma=0.0005$ eV. In this model about 90% of the oscillator strength is in the transition to ω_-.

We shall distinguish between three typical cases which differ by the detuning of ω_1 and ω_2: (1) Both frequencies are tuned far off-resonant from any one-exciton transition. (2) ω_1 is in the vicinity of a one-exciton transition and ω_2 is tuned across one- and two-exciton resonances. (3) ω_1 is in resonance with a one-exciton transition and ω_2 is tuned across one- and two-exciton resonances. In Fig. 3 we display W_{TPA} for these cases in the two-level limit ($\kappa_n=0$). In panel (a) we show case (1) which yields excited state absorption due to a transition from a one- to the two-exciton state at energy $\omega_++\omega_-$. If ω_1 approaches a one-exciton resonance, $\omega_1\rightarrow\omega_-$ in Figs. 3(b) and 3(c) [case (2)], W_{TPA} shows a dispersive feature as ω_2 is scanned through a one-exciton resonance and excited state absorption if $\omega_1+\omega_2=\omega_++\omega_-$. Note that when ω_1 is tuned within the linewidth of the one-exciton transition, one- and two-photon resonances strongly interfere [Fig. 3(c)]. If ω_1 is on resonance with a one-exciton transition [case (3)] this interference leads to

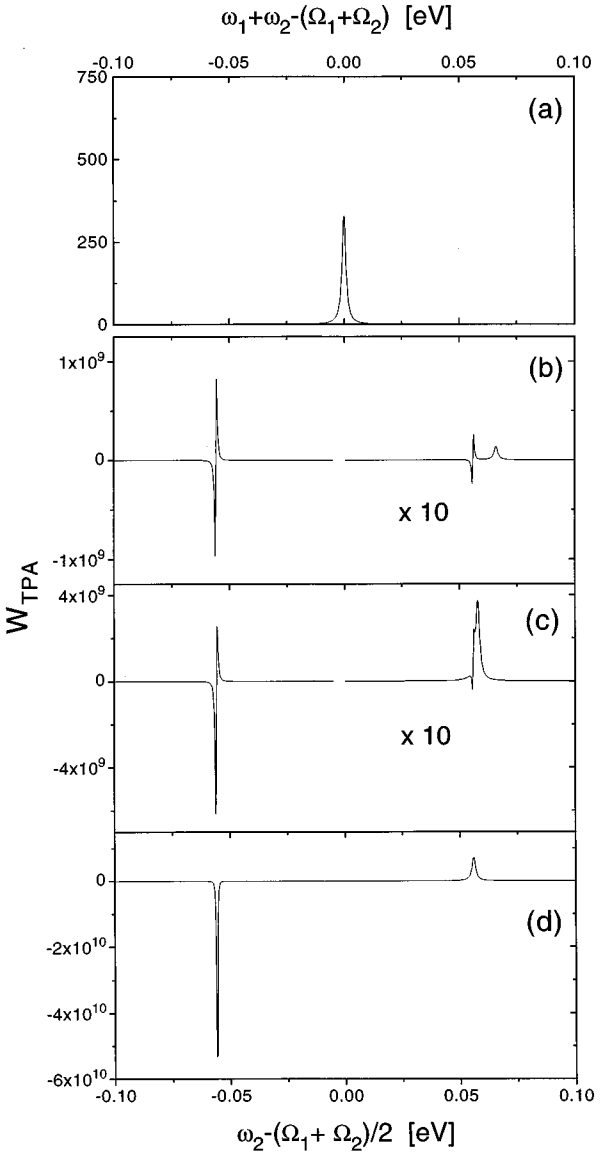

FIG. 3. The two-photon absorption signal, W_{TPA}, calculated for a dimer made of two-level molecules using different detunings. (a) $\hbar\omega_1=1$ eV [case (1)], (b) $\hbar\omega_1=\omega_--0.01$ eV, (c) $\hbar\omega_1=\omega_--0.002$ eV, and (d) $\hbar\omega_1=\omega_-$. The other parameters are $\hbar\Omega_1=1.475$ eV, $\hbar\Omega_2=1.525$ eV, $J_{12}=-0.05$ eV, and $\hbar\Gamma=5\times10^{-4}$ eV.

Downloaded¬08¬Mar¬2001¬to¬128.151.176.185.¬Redistribution¬subject¬to¬AIP¬copyright,¬see¬http://ojps.aip.org/jcpo/jcpcpyrts.html

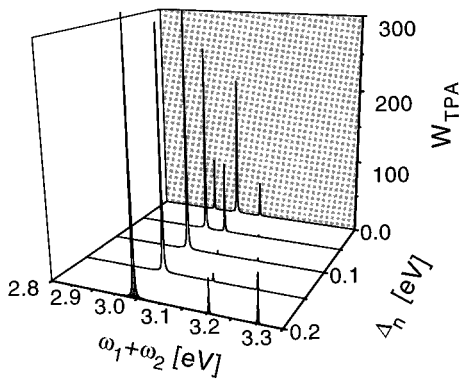

FIG. 4. The same as Fig. 3(a) but for the three-level case using different values of the anharmonicity Δ_n ($\kappa_1=\kappa_2=0.5$).

saturated absorption for $\omega_2=\omega_-$ and an excited state absorption for $\omega_2=\omega_+$, as seen in Fig. 3(d).

If a third intramolecular level is taken into account, two additional two-photon resonances become possible. These are conveniently investigated in case (1). In Fig. 4 we choose $\hbar\omega_1=1$ eV and tune ω_2 across the two-exciton band. Figure 4a shows the dependence of W_{TPA} on the anharmonicity Δ_n for $\kappa_n=0.5$. For small Δ_n there is a strong mixing between the CDE at $\hbar(\omega_1+\omega_2)=\hbar(\omega_++\omega_-)=3$ eV for $\kappa_n=0$ and the two MDE's. Increasing the anharmonicity, Δ_n, reduces the coupling between intra- and intermolecular two-photon resonances, and for $\Delta_n \gg \kappa_n J_{12}$ one obtains independent peaks due to excited state absorption at $\omega_1+\omega_2=\omega_++\omega_-$ and $\hbar(\omega_1+\omega_2)=2\hbar\Omega_{n=1,2}+\Delta_{n=1,2}$.

In Fig. 5(a) we display W_{TPA} as a function of κ_n for $\Delta_n=0$. The splitting between the peaks increases with κ_n and is symmetric with respect to the resonance at $\omega_++\omega_-$. The origin of the asymmetric distribution of oscillator strength between the three peaks can be traced by looking at the different contributions which interfere to give the third-order susceptibility. In Fig. 5(b) we show the spectrum which results from the scattering matrix only (setting all single exciton Green's functions equal to 1) while Fig. 5(c) shows the spectrum which results from the one-exciton Green's functions only [setting $\overline{\Gamma}_{\alpha_1\alpha_2,\alpha_3\alpha_4}(\omega)=1$ in Eq. (3.21)].

The third-order response vanishes for $\kappa_n=\sqrt{2}$ and $\Delta_n=0$ (harmonic system) as shown in Fig. 5(a). This property leads to a reduction of the TPA-signal in the vicinity of $\kappa_n=\sqrt{2}$ even if a small anharmonicity is introduced. This can be seen in Fig. 6 where we put $\Delta_n=0.05$ eV.

We next focus attention on case (2) where ω_1 is off-resonant with respect to $\omega_\pm$ and ω_2 is tuned through one- and two-exciton resonances. In Fig. 7(a) we show W_{TPA} as a function of ω_2 for $\hbar\omega_1=1.43$ eV, $\Delta_n=0.1$ eV, and $\kappa_n=1$. In addition to the three two-photon resonances we observe dispersive resonances when ω_2 is tuned across the one-exciton transitions. For comparison we show in panel (b) W_{TPA} calculated using the LFA for the scattering matrix. The LFA only accounts for the dispersive features as well as for

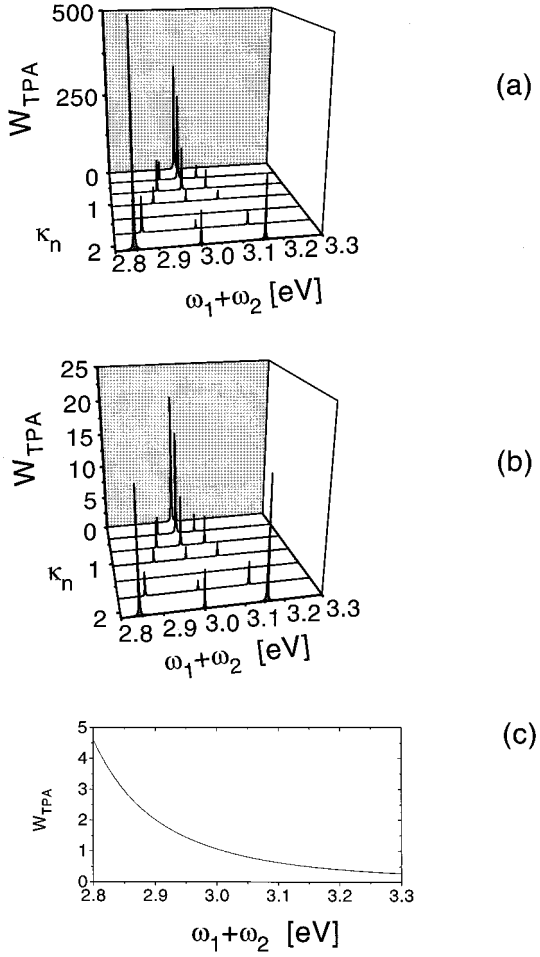

FIG. 5. The same as Fig. 3(a) but for the three-level case using different values of κ_n ($\Delta_n=0$): (a) full calculation [Eq. (3.21)], (b) exciton scattering matrix only, and (c) Green's function only (see the text).

the two MDE's [see Eq. (3.16)]. From Eq. (3.16) it follows further that these peaks do not shift as κ_n is varied. In other words, all information about the coupling between MDE and CDE is lost in this approximation.

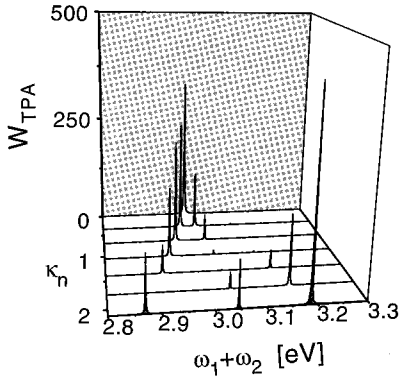

FIG. 6. The same as Fig. 5(a) but for $\Delta_n=0.05$ eV.

Downloaded¬08¬Mar¬2001¬to¬128.151.176.185.¬Redistribution¬subject¬to¬AIP¬copyright,¬see¬http://ojps.aip.org/jcpo/jcpcpyrts.html

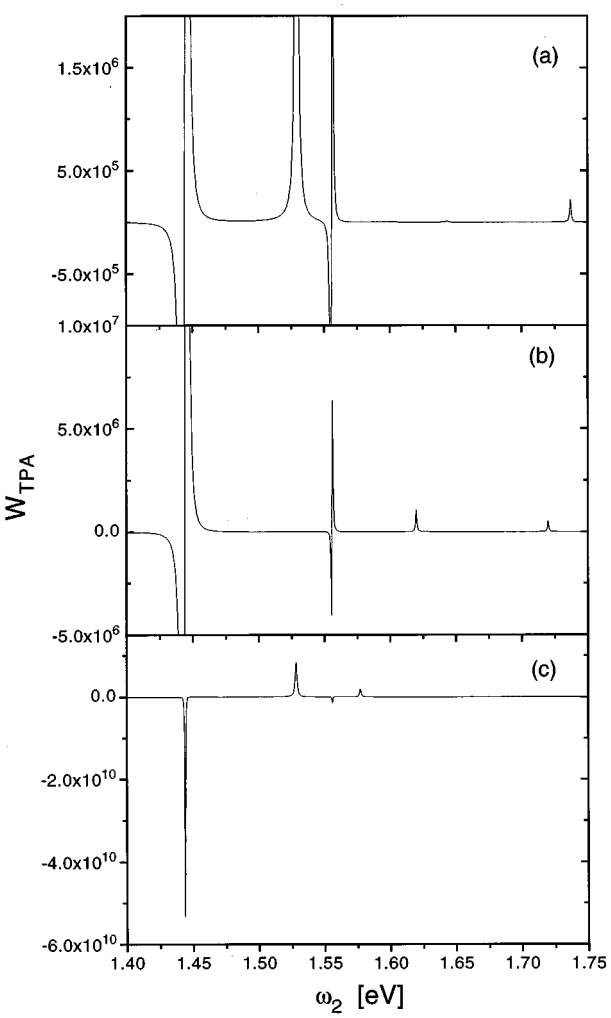

FIG. 7. W_{TPA} for a three-level dimer with anharmonicity $\Delta_n=0.1$ eV and $\kappa_n=1$: (a) full calculation for off-resonant excitation ($\hbar\omega_1=1.43$ eV) and (b) local field approximation [Eq. (3.16)]. In panel (c) we show the full calculation for resonant excitation ($\omega_1=\omega_-$), $\Delta_n=0.05$ eV, and $\kappa_n=0.5$ (other parameters are as in Fig. 3).

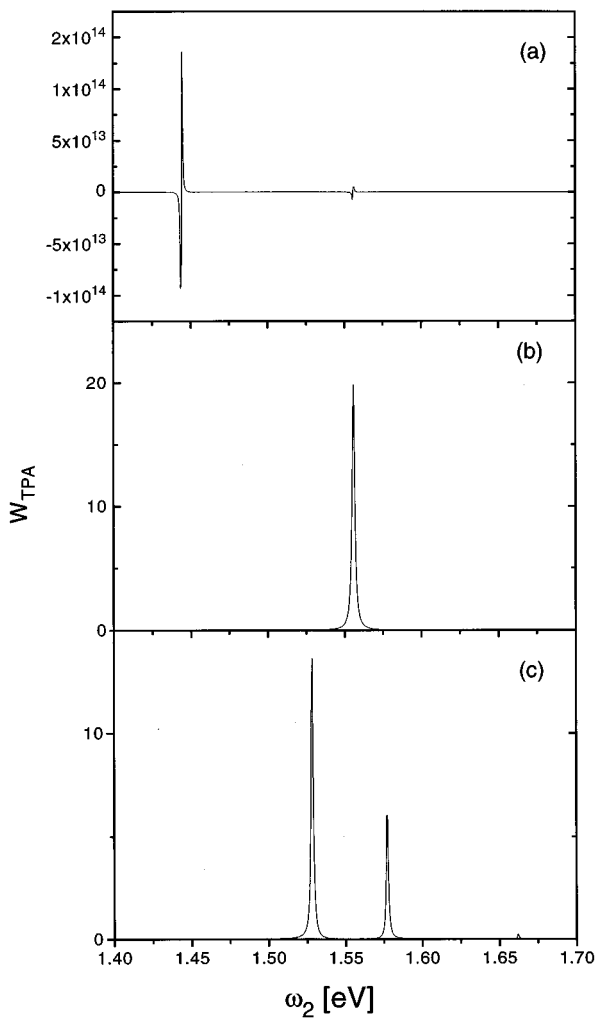

FIG. 8. Decomposition of W_{TPA} shown in Figs. 3(d) and 7(c): (a) Green's functions only, (b) scattering matrix only (two-level limit), and (c) scattering matrix only ($\Delta_n=0.05$ eV and $\kappa_n=0.5$).

Finally, we investigate the resonance case (3) for $\omega_1=\omega_-$. In Fig. 7(c) we calculated W_{TPA} for a three-level system with $\kappa_n=0.5$ and $\Delta_n=0.05$ eV. If one- and two-photon resonances exist for similar frequencies of the probe beam, as it is the case in Figs. 7a and 7c, it is desirable to look at the different contributions to the spectrum. Figure 8 shows the spectrum calculated when only the four Green's functions are included in Eq. (3.21) and the scattering matrix is set equal to 1 [panel (a)] together with the contribution of the scattering matrix only [panels (b) and (c)]. The Green's function contribution always gives dispersive features regardless of the pump and probe frequencies. Obviously only the interference with the complex exciton scattering matrix leads to the negative absorption peak at $\omega_1=\omega_2=\omega_-$ (saturated absorption) and the excited state absorption at $\omega_2=\omega_+$ in the two-level limit [panel (b)]. In the three-level case the two-photon resonances due to the scattering matrix no longer show up at $\omega_1+\omega_2=\omega_++\omega_-$ for the present parameters. This is a consequence of the interaction between MDE and CDE. Thus we observe a saturated absorption peak at $\omega_2=\omega_+$. This convenient way of interpreting the different resonances in terms of the Green's function and the exciton scattering matrix is very different from the more common SOS-approach which requires the knowledge of all transition energies and dipole matrix elements [see, Eq. (3.24)].

Having considered the spectra for different pump and probe frequencies in the case of a dimer we are now in the position to investigate the more complex antenna aggregates.

B. LH2 of purple bacteria

In the following we apply the results of Section II to the outer antenna of photosynthetic bacteria. We will focus on *Rps. acidophila* for which the geometry of the LH2 is known to high precision.[3] However, it is commonly believed that the LH2s of other systems, such as the widely studied *Rb. sphaeroides*, are organized in a similar way.

Electron diffraction from crystals of the LH2 complex of *Rps. acidophila*[3] revealed 27 BChl *a*'s, 18 of which are situ-

Downloaded¬08¬Mar¬2001¬to¬128.151.176.185.¬Redistribution¬subject¬to¬AIP¬copyright,¬see¬http://ojps.aip.org/jcpo/jcpcpyrts.html

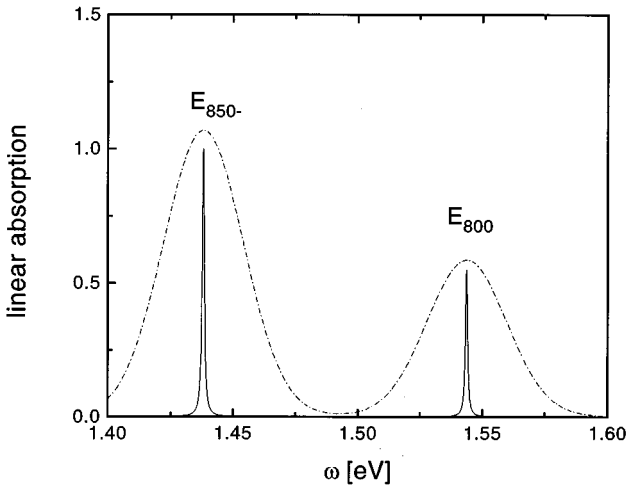

FIG. 9. Linear absorption spectrum, Im $\chi^{(1)}(-\omega;\omega)$, for the LH2 complex for the case of lifetime broadening only ($\hbar\Gamma=5\times10^{-4}$ eV) (a), and after convolution with a single Gaussian (FWHM 0.0372 eV). (b) The interaction energies and the transition frequencies for the B800 and the B850 band have been taken from Ref. 5.

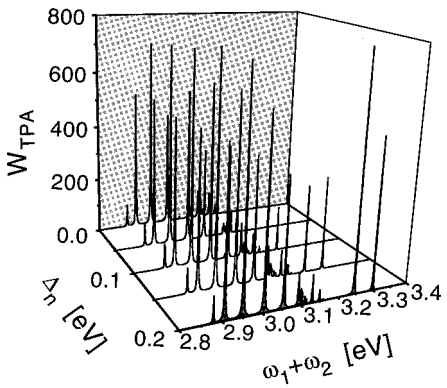

FIG. 10. Dependence of the W_{TPA}-signal from the two-exciton band on the anharmonicity for $\kappa_n=0.5$ in LH2 ($\hbar\omega_1=1$ eV, $\hbar\Gamma=5\times10^{-4}$ eV).

ated on the rim of an inner ring and the remaining 9 molecules form an outer ring. The Q_y-transitions of the BChl *a*'s on the outer (inner) ring are responsible for the higher (lower) energetic absorption band [B800 (B850) in *Rb. sphaeroides*, for instance]. On the basis of these data Sauer *et al.*[5] recently calculated the interaction energies, J_{mn}, between different molecules using point–monopole transition moments and suggested two distinct S_0-S_1 transition energies for the B800 ($\hbar\Omega_{800}=1.55$ eV) and the B850 ($\hbar\Omega_{850}=1.52024$ eV) molecules, respectively. The resulting parameters give a reasonable fit to the linear absorption spectrum of *Rps. acidophila* after convoluting the excitonic stick spectrum with a single Gaussian of 0.0372 eV FWHM representing line broadening. In the following we will use these parameters in our calculations of the nonlinear optical response. In the numerical simulations we will vary the anharmonicity, Δ_n, and the the ratio between the transition dipole moments, κ_n, assuming that the latter are parallel. It should be mentioned that estimates of these quantities have only recently been proposed on the basis of time-resolved pump-probe data.[16]

In Fig. 9 we show the linear absorption spectrum, Im $\chi^{(1)}(-\omega_1;\omega_1)$. The spectrum shows two peaks which can be assigned to the outer ring (E_{800}) as well as to the lowest (E_{850-}) state of the inner ring one-exciton band. The highest (E_{850+}) state of the inner ring one-exciton band which is at about 1.58 eV also carries oscillator strength but cannot be resolved on this scale.[25] The spectrum after convolution with a single Gaussian (FWHM 0.0372 eV) is plotted as a dash–dotted line in Fig. 9. The fact that only three excitonic transitions account for most of the oscillator strength of the system results in a considerable reduction of numerical effort. The sum over the N exciton oscillators in Eq. (3.21) can be restricted to these essential oscillators by introducing a cutoff for μ_α. We have checked numerically that this truncation leads only to a slight overall reduction of the magnitude of the TPA.

We first investigate the structure of the two-exciton band using case (1) of Fig. 3 in which no one-exciton resonances are involved. For simplicity we hereafter use the same Δ_n and κ_n for all monomers. In Fig. 10 we show the variation of W_{TPA} with anharmonicity for $\kappa_n=0.5$. As in the dimer case the intramolecular $S_1\rightarrow S_2$ transitions become well separated from the two-exciton band as Δ_n is increased, i.e. the interaction between MDE and CDE is reduced. Note, that there are only two distinct intramolecular resonances on the blue side of the spectrum since in the present model of the LH2 there are only two different monomer transition energies. In Fig. 11 we display the dependence of W_{TPA} on κ_n for zero anharmonicity [panel (a)] and for $\Delta_n=0.05$ eV [panel (b)]. First we notice that the response completely vanishes for $\kappa_n=\sqrt{2}$ and $\Delta_n=0$ and that it is considerably reduced for $\kappa_n=\sqrt{2}$ and $\Delta_n=0.05$ eV. More striking, however, is the fact that in both cases with increasing κ_n the oscillator strength for two-photon absorption accumulates in the band edges of the two-exciton band. This effect can be attributed to the circular symmetry of the LH2 and it does not show up in the less symmetric LHC-II as we will see shortly. Finally, it should be mentioned that W_{TPA} in Figs. 10 and 11 reflects the behavior of the exciton scattering matrix. The contributions due to the Green's functions show no resonances similar to that of the dimer (Fig. 5).

Next we tune ω_1 in the vicinity of a one-exciton transition. Here we focus on the highest exciton state of the B850 band, E_{850+}. So far there is no experimental evidence for the existence of an optically active state E_{850+}, which could allow us to determine the overall bandwidth of the one-exciton manifold. This in turn should provide a test for theoretical calculations of the intermolecular coupling strengths. We have verified that the oscillator strength for this transition vanishes if the coupling matrix, J_{mn}, given in Ref. 5 is modified as follows: There is only nearest neighbor interaction within the inner ring and the coupling between the inner and the outer ring is turned off.

In order to find signatures of the E_{850+} state in the TPA-

Downloaded¬08¬Mar¬2001¬to¬128.151.176.185.¬Redistribution¬subject¬to¬AIP¬copyright,¬see¬http://ojps.aip.org/jcpo/jcpcpyrts.html

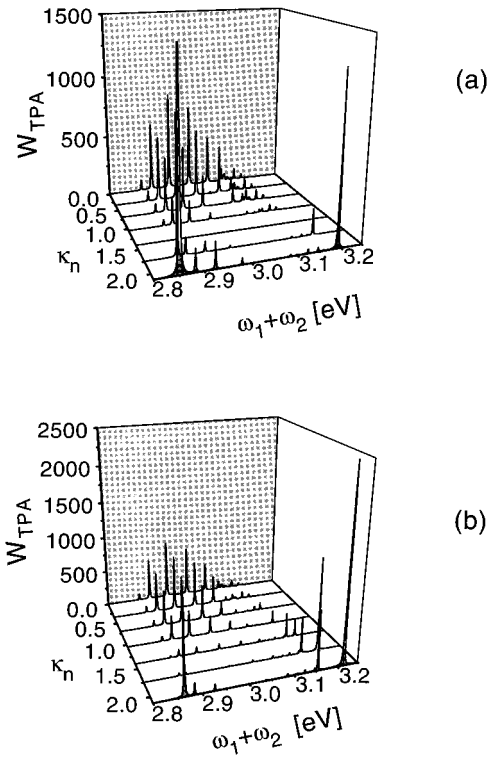

FIG. 11. Same as in Fig. 10 but for different κ_n; (a) $\Delta_n=0$ and (b) $\Delta_n=0.05$ eV.

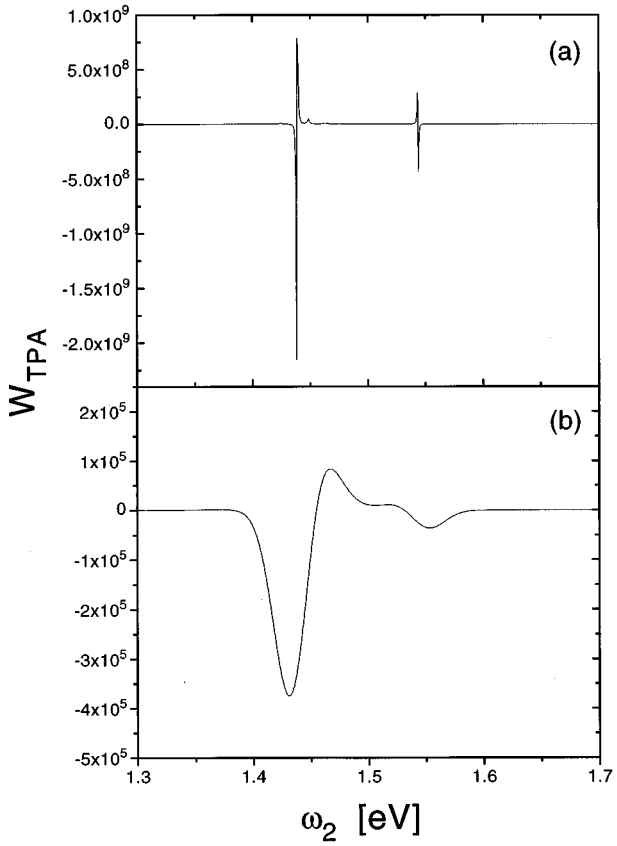

FIG. 12. LH2 W_{TPA}-signal for resonant excitation at $\hbar\omega_1=E_{850+}$ in the two-level limit [(a) only lifetime broadening ($\hbar\Gamma=5\times10^{-4}$ eV), (b) convolution with single Gaussian (FWHM 0.0372 eV)].

signal we have calculated W_{TPA} for $\hbar\omega_1=E_{850+}=1.581$ eV (Fig. 12) and for $\hbar\omega_1=1.6$ eV (Fig. 13) in the two-level limit. The upper panels include the phenomenological lifetime broadening only, and in the lower panels the spectrum has been convoluted with a single Gaussian (0.0372 eV FWHM) to account for inhomogeneous broadening. In both figures the resonance features around E_{850+} cannot be resolved on this scale since the response in the vicinity of E_{800} and E_{850-} is much stronger. Nevertheless, the curves are remarkably different. For resonant excitation the correlation between the highest and the lowest state of the B850 band leads to a negative absorption at E_{850-} and two rather strong excited state absorption peaks on the blue side of this state. The feature at E_{800} is dispersive due to the rather weak coupling between the inner and the outer ring, i.e. there is no strong two-exciton transition close to E_{800} for this setup. For off-resonant excitation the response at E_{800} and at E_{850-} is dispersive. This totally different behavior persists when line broadening is included [Figs. 12(b) and 13(b)].

In Figs. 14 and 15 we used the same excitation conditions but included $S_1\rightarrow S_2$ transitions with $\Delta_n=0.05$ eV and $\kappa_n=2$. As in the two-level case, the existence of an optically active state, E_{850+}, strongly affects the TPA-signal if the pump beam is tuned on resonance with this transition. More interesting, however, is the fact that the incorporation of higher intramolecular transitions results in strong excited state absorption in between E_{850-} and E_{800} and on the blue side of E_{800} [compare the broadened spectra in Figs. 12(b)–15(b)]. The latter feature is reminiscent of the redistribution of oscillator strength for two-photon absorption seen in Fig. 11, even though the situation is more complex here due to the interference with the one-exciton transitions.

C. LHC–II of green plants

We next focus attention on the LHC-II which lacks the high symmetry of the LH2 system. Spectroscopic investigations (e.g., electroabsorption[26]) indicate that there are several distinct one-exciton transitions contributing to the absorption spectrum. The low resolution of the structural data[2] does not allow an unambiguous identification of the Chl *a* and Chl *b* molecules or an assignment of the respective orientations of the transition dipole moments. The functionality of the LHC-II, however, suggests the chlorophylls closest to the carotenoids to be Chl *a* (7), while the remaining are Chl *b* (5). Using this assignment, the low temperature absorption spectrum has been successfully simulated using the methods developed in Ref. 27, and assuming the transition dipoles to be parallel to the membrane plane.[28] In contrast to a perpendicular arrangement, this configuration was shown[29] to reproduce the correct behavior of the ultrafast transient absorption reported in Ref. 11. This is also in accord with polarized absorption and fluorescence studies which gave an average orientation of the transition dipoles within the Chl *a* domi-

Downloaded¬08¬Mar¬2001¬to¬128.151.176.185.¬Redistribution¬subject¬to¬AIP¬copyright,¬see¬http://ojps.aip.org/jcpo/jcpcpyrts.html

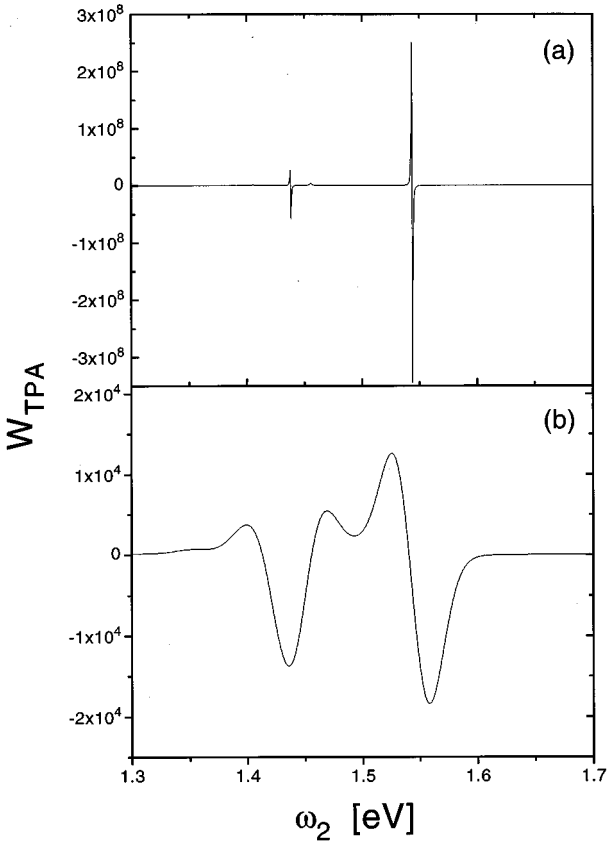

FIG. 13. The same as in Fig. 12 using off-resonant excitation at $\hbar\omega_1 = 1.6$ eV.

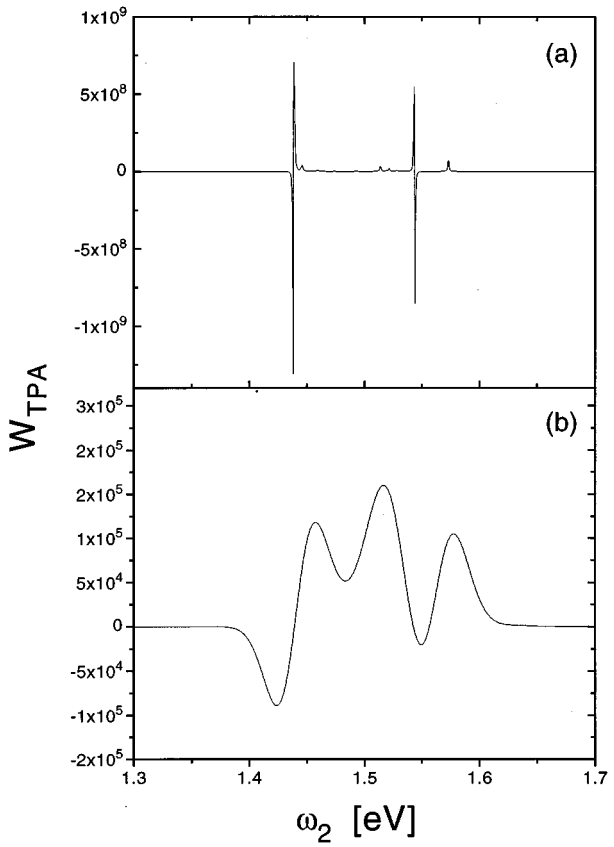

FIG. 14. The same as in Fig. 12 but for three-level molecules ($\Delta_n = 0.05$ eV, $\kappa_n = 2$).

nated band at 676 nm of about 12° with respect to the membrane plane. For the Chl *b* dominated band at 640 nm this angle was found to be about 35°.[30] It should be noted that an attempt has been made recently to assign orientations to the individual chlorophylls based on a modeling of linear and circular dichroism spectra.[31] So far, however, this rather complicated task gave only unambiguous information about the orientation of three out of the twelve chlorophyll molecules. Possible orientations of the remaining molecules have been inferred from ultrafast pump-probe measurements.[14]

Concerning the $S_1 \rightarrow S_2$ transition, the available informations indicate a rather strong Chl *a* singlet excited state absorption (MDE) for wavelengths in the region of Chl *b* $S_0 \rightarrow S_1$ transitions in LHC-II.[11,14,17,32] However, in order to explore the principal effects of MDE in non-symmetric aggregates like the LHC-II we will vary Δ_n and κ_n over a broad range, assuming the same values for all monomers.

Figure 16 shows the linear absorption according to Ref. 28 of the LHC-II without (solid line) and with inclusion of inhomogeneous broadening [convolution of the total spectrum with a single Gaussian (FWHM 0.0186 eV), dash–dotted line]. Compared with the LH2 (Fig. 9) the spectrum has a much richer structure with ten distinct exciton transitions. The two main peaks in the broadened spectra are dominated by Chl *b* (blue side) and Chl *a* (red side) molecules. In Fig. 17 we calculated W_{TPA} in the two-exciton regime as a function of the anharmonicity for $\kappa_n = 0.5$. As in the previous model systems, the intramolecular $S_1 \rightarrow S_2$ transitions show up as distinct excited state absorption peaks on the blue side of the band if Δ_n increases. Note that there are only seven distinct peaks since some monomer transitions energies are assumed to be equal in the present simulation (see the caption to Fig. 16). The behavior of W_{TPA} upon increasing the ratio κ_n if Δ_n is fixed is shown in Fig. 18 [$\Delta_n = 0$ panel (a), $\Delta_n = 0.05$ eV panel (b)]. Besides the expected greater complexity compared with the corresponding LH2 spectra, W_{TPA} for LHC-II is different in two respects: First, for the same value of Δ_n the signal does not show the strong reduction in magnitude for $\kappa_n = \sqrt{2}$ (compare, Figs. 11b and 18b). Second, there are no signatures for an accumulation of all oscillator strength in the edges of the two-exciton band, as was the case in the highly symmetric LH2.

Finally, we show the TPA-signal in the two-level limit (Fig. 19) and for a three-level system (Fig. 20). The frequency ω_1 is tuned in resonance with the highest state of the one-exciton manifold ($\hbar\omega_1 = 1.916$ eV) which is due to Chl *b*. In both figures the spectra show four strong absorptive peaks. Three are in the Chl *b* region and the fourth is positioned at the main peak of the Chl *a* absorption band. This indicates the relatively strong coupling between some pigments in the Chl *b* pool and between the highest state in the

Downloaded¬08¬Mar¬2001¬to¬128.151.176.185.¬Redistribution¬subject¬to¬AIP¬copyright,¬see¬http://ojps.aip.org/jcpo/jcpcpyrts.html

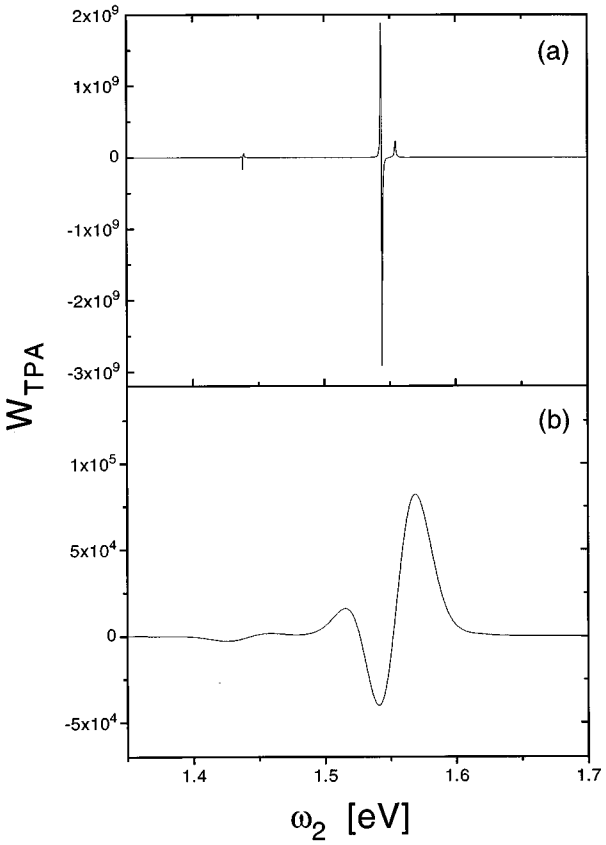

FIG. 15. The same as in Fig. 13 but for three-level molecules ($\Delta_n=0.05$ eV, $\kappa_n=2$).

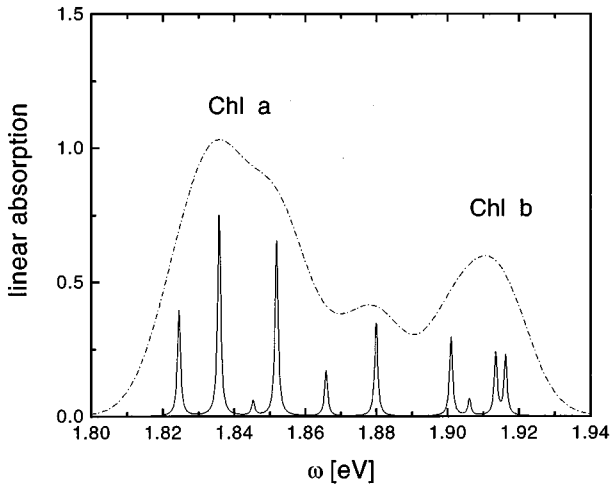

FIG. 16. Linear absorption spectrum of the LHC-II calculated with the interaction energies estimated in Ref. 28 for transition dipoles oriented parallel to the membrane plane. Panel (a) shows the stick spectrum while in panel (b) the data have been convoluted with a single Gaussian [FWHM 0.0186 eV (150 cm^{-1}) ($\hbar\Gamma=5\times10^{-4}$ eV]. For the monomer transition energies of the different chlorophyll molecules the following values have been used (nomenclature as in Ref. 2) $E_{a1}=E_{a2}=E_{a4}=1.843$ eV, $E_{a3}=1.858$ eV, $E_{a5}=1.828$ eV, $E_{a6}=1.867$ eV, $E_{a7}=1.879$ eV, $E_{b1}=E_{b2}=1.913$ eV, $E_{b3}=E_{b5}=E_{b6}=1.9$ eV. The strongest interaction energies ($|J_{mn}|>5$ meV) are $J_{a1,a2}=-5.5$ meV, $J_{a1,b1}=-12.7$ meV, $J_{a2,b2}=-5.6$ meV, $J_{a3,b3}=-17.2$ meV, $J_{a4,b5}=-6.9$ meV, $J_{a5,b5}=-6.1$ meV. For the dipole strengths of the monomers $\mu_a^2=15.5$ D^2 and $\mu_b^2=12.5$ D^2 has been used.[28]

Chl *b* dominated band and Chl *a* molecules. The inclusion of a third intramolecular level ($\Delta_n=0.025$ eV and $\kappa_n=1$) yields a strong excited state absorption to the blue of the Chl *b* absorptive feature [compare broadened spectra in panels (c)]. The contribution to the susceptibility of the exciton scattering matrix only is shown in panels (b). It indicates the positions of two-photon resonances. Their magnitudes are affected by the interference with the one-exciton Green's functions.

V. SUMMARY

The formulation of the nonlinear optical response using coupled anharmonic excitonic oscillators provides a powerful tool for the study of large aggregates. The third-order susceptibility can be expressed in terms of one-exciton Green's functions and an $N\times N$ exciton scattering matrix. This is a clear advantage compared with the conventional sum-over-states approach which requires the calculation of $2N+(N-1)N/2$ eigenstates and the corresponding transition dipole matrix elements. It further allows a semiclassical interpretation of optical spectra in terms of free motion and scattering processes of excitons.

The formalism has been applied to the calculation of frequency-domain two-photon absorption spectra of light-harvesting antenna complexes possessed by purple bacteria and green plants. The LH2 and the LHC-II are structurally very different; this is reflected in the third-order response. The parameters in our calculation, such as the anharmonicity and the ratio between the $S_1\rightarrow S_2$ and the $S_0\rightarrow S_1$ have been chosen to highlight possible scenarios. Under certain conditions we predict the accumulation of oscillator strength in the two-photon transitions to the edges of the two-exciton band in LH2 and that the manifestations of the E_{850+} state are experimentally observable. Even though the quality of structural information about the antenna systems is rapidly improving, simulations of linear absorption and circular or lin-

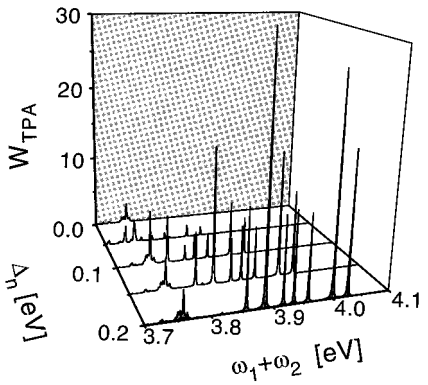

FIG. 17. The same as in Fig. 10 but for LHC-II.

Downloaded¬08¬Mar¬2001¬to¬128.151.176.185.¬Redistribution¬subject¬to¬AIP¬copyright,¬see¬http://ojps.aip.org/jcpo/jcpcpyrts.html

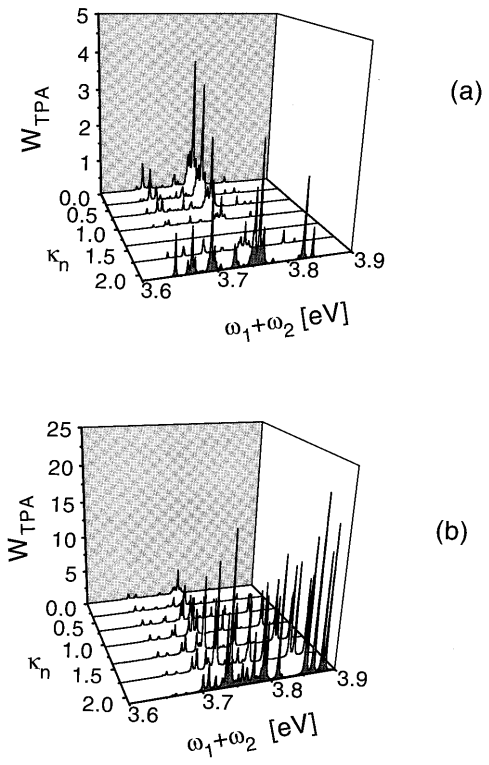

FIG. 18. The same as in Fig. 11 but for LHC-II.

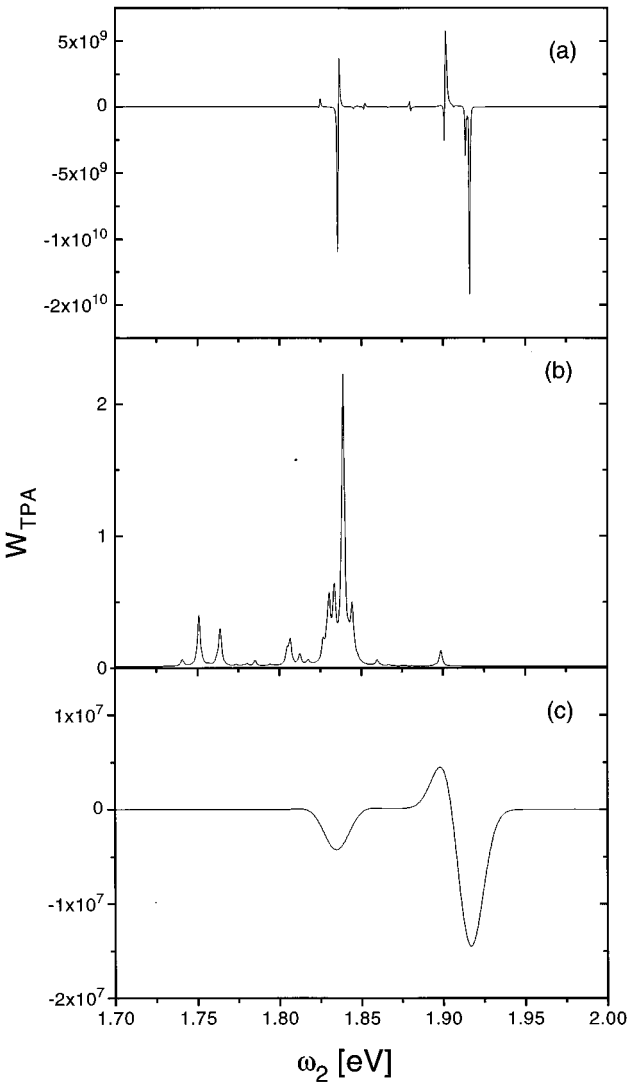

FIG. 19. TPA-signal for LHC-II using resonant excitation at $\hbar\omega_1 = 1.916$ eV (highest one-exciton state) in the two-level limit [(a) only lifetime broadening, (b) contribution due to the exciton scattering matrix only, (c) convolution with single Gaussian (FWHM 0.0186 eV)].

ear dichroism spectra based on the refined geometry are only recently coming out. In particular only few studies on the singlet excited state absorption of chlorophyll molecules in the antenna complex have been reported.[14,16,17,32]

The time-resolved signals in the pump-probe setup at low temperature[33] as well as the room temperature photon echo and transient grating data[8] show a clear evidence for a coupling of the excitation energy transfer to nuclear vibrational modes of the BChl *a* monomers and of the pigment-protein complex in the LH2. Room temperature vibrational quantum beats have also been found in other complex biological systems such as the photosynthetic reaction center of purple bacteria.[34] There are no observations of quantum beats due to vibrational motion for the LHC-II yet. From the theoretical point of view, a complete description of the coupled exciton-vibrational dynamics in large aggregates is an extremely challenging task. Using an approach based on the reduced density matrix formulated in localized exciton-vibrational eigenstates it was shown that the exact treatment of a dimer including one nuclear degree of freedom per monomer approaches the limits of present computers.[29,35] The restriction to a few relevant excitonic variables reduces the number of equations of motion compared with a full density matrix description considerably. Even though there are schemes to incorporate weak exciton–phonon coupling into this formalism[22] a theory which is capable of accounting for strong coupling in large aggregates is yet to be developed.

ACKNOWLEDGMENTS

We wish to thank Professor K. Sauer for making Ref. 5 available to us prior to publication. This work was supported by the National Science Foundation and the Air Force Office of Scientific Research. O. K. gratefully acknowledges a postdoctoral fellowship from the German Academic Exchange Service (DAAD).

APPENDIX A: DEFORMED BOSON REPRESENTATION OF MULTI–LEVEL MOLECULES

We consider an aggregate made of molecules with a ground state and M excited states. We further assume that all molecular transition dipoles are parallel and the only nonzero transition dipole matrix elements are between adjacent levels, i.e. $|f_n)$ and $|f_n \pm 1)$. For simplicity we neglect line broadening in the following derivation.

Downloaded¬08¬Mar¬2001¬to¬128.151.176.185.¬Redistribution¬subject¬to¬AIP¬copyright,¬see¬http://ojps.aip.org/jcpo/jcpcpyrts.html

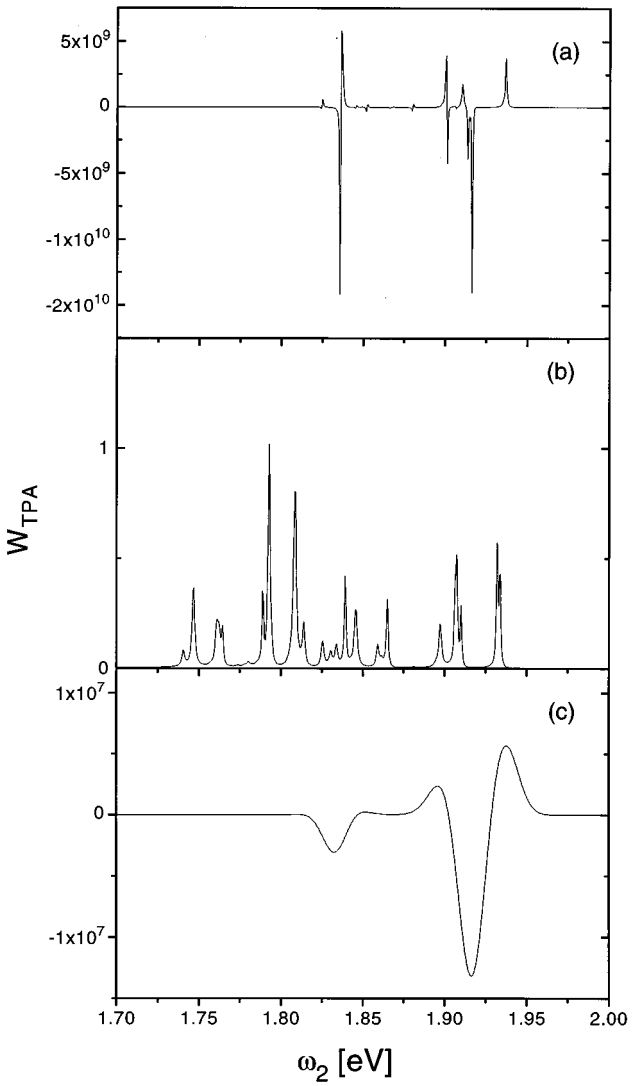

FIG. 20. The same as in Fig. 19 but for three-level molecules ($\Delta_n=0.025$ eV, $\kappa_n=1$).

The Hamiltonian has the form

$$H=\sum_n H_n+\sum_{mn}\beta_{mn}d_m d_n, \tag{A1}$$

where β_{mn} is given by Eq. (2.6). H_n is the single molecule Hamiltonian

$$H_n=\sum_{f=0}^{M}\hbar\Omega_n^{(f)}|f_n)(f_n|, \tag{A2}$$

and d_n is the molecular dipole operator

$$d_n=\sum_{f=0}^{M-1}[\mu_n^{(f,f+1)}|f_n)(f_n+1|+\mu_n^{(f+1,f)}|f_n+1)(f_n|]. \tag{A3}$$

The three-level Frenkel Hamiltonian used in Section II [Eqs. (2.3) and (2.4)] is a special case of Eqs. (A1)–(A3). It has been shown in Refs. 36 and 37 that there are two ways to distinguish between effects of statistics and anharmonicity in optical nonlinearities. One way is to represent the system Hamiltonian in terms of operators with boson commutation relations. This is known as bosonization.[38–43] Effects of statistics then give nonlinear terms in the expansion of the polarization operator in powers of the boson variables. This approach, however, has a major difficulty since one needs to follow the evolution of expectation values of products of boson operators in order to get the observable (e.g., the polarization). It is therefore preferable to find a representation in which the polarization operator is linear in elementary variables, effects of statistics then show up in non-boson commutation relations of the basic operators. To accomplish this goal for the system described by Eqs. (A1)–(A3), we first write the molecular dipole operator d_n as

$$d_n=\mu_n(B_n+B_n^\dagger), \tag{A4}$$

where $\mu_n=\mu_n^{(10)}$ and

$$B_n^\dagger=\sum_{f=0}^{M-1}\frac{\mu_n^{(f+1,f)}}{\mu_n}|f_n+1)(f_n|,$$
$$B_n=\sum_{f=0}^{M-1}\frac{\mu_n^{(f,f+1)}}{\mu_n}|f_n)(f_n+1|. \tag{A5}$$

According to Eq. (A4) the polarization operator is linear in the B_n and $B_n^\dagger$ operators. The second term of the Hamiltonian, given by Eq. (A1), is expressed naturally in terms of these operators. We now need to find the single molecule Hamiltonian in terms of the B_n and $B_n^\dagger$ operators and to calculate their commutation relations. This can be done by applying the procedure of Ref. 36. Making use of the fact that the operators $[B_m,B_n^\dagger]$ and H_n are diagonal in the basis set of $|f_n)$, we can represent them in the form

$$H_n=\sum_{f=1}^{M}\frac{1}{f!}\hbar\omega_n^{(f)}(B_n^\dagger)^f(B_n)^f, \tag{A6}$$

$$[B_m,B_n^\dagger]=\delta_{mn}\left[1-\sum_{f=1}^{M-1}q_n^{(f)}(B_n^\dagger)^f(B_n)^f\right]. \tag{A7}$$

Equation (A7) represents commutation relations of operators B_n and $B_n^\dagger$ Substituting Eqs. (A4) and (A6) into Eq. (A1) we recast the Hamiltonian in terms of the operators B_n and $B_n^\dagger$ To obtain the coefficients $\omega_n^{(f)}$ and $q_n^{(f)}$ in the expansion of Eqs. (A6) and (A7) we evaluate the matrix elements of the operators $[B_m,B_n^\dagger]$ and H_n using Eqs. (A2)–(A4) and compare them with those obtained by using Eqs. (A5)–(A7). The coefficients $q_n^{(f)}$ can be determined recursively:

$$\left[\frac{\mu_n^{(f+1,f)}}{\mu_n}\right]^2-\left[\frac{\mu_n^{(f,f-1)}}{\mu_n}\right]^2=1-\sum_{s=1}^{f}q_n^{(s)}\prod_{p=f-s}^{f-1}\left[\frac{\mu_n^{(p+1,p)}}{\mu_n}\right]^2. \tag{A8}$$

The parameters $\omega_n^{(f)}$ can be obtained from

Downloaded¬08¬Mar¬2001¬to¬128.151.176.185.¬Redistribution¬subject¬to¬AIP¬copyright,¬see¬http://ojps.aip.org/jcpo/jcpcpyrts.html

$$\frac{1}{f!}\omega_n^{(f)}\prod_{s=1}^{f-1}\left[\frac{\mu_n^{(s+1,s)}}{\mu_n}\right]^2=\Omega_n^{(f)}-\sum_{s=1}^{f-1}\omega_n^{(s)}\prod_{p=f-s}^{f-1}\left[\frac{\mu_n^{(p+1,p)}}{\mu_n}\right]^2. \tag{A9}$$

In the case of a three-level system, Eqs. (A8) and (A9) give $q_n^{(1)}=2-\kappa_n^2$, $\Omega_n^{(1)}=\omega_n^{(1)}$, and $\Omega_n^{(2)}=\kappa_n^2(\omega_n^{(1)}+\omega_n^{(2)}/2)$. These results have been used in Section II ($\hbar\omega_n^{(2)}=g_n$).

APPENDIX B: TIME–DOMAIN RESPONSE

In this appendix we derive the equations of motion including the one- and two-exciton variables for calculating a general nonlinear optical response induced by M laser pulses. The external field is expanded as

$$E_n(t)=\sum_{j=1}^{M}E_n^{(j)}(t)e^{i\vec{k}_j\vec{r}_n}, \tag{B1}$$

where $E_n^{(j)}(t)=\mu_n A_j(t)\exp\{-i\omega_j t\}$ with $A_j(t)$ being the envelope of the jth pulse.

In order to distinguish between the different directions of the signal we follow Ref. 44 and expand all dynamical variables as

$$X=\sum_{\alpha_1,\ldots,\alpha_M=-\infty}^{\infty}X^{(\alpha_1,\ldots,\alpha_M)}\times\exp\{i(\alpha_1\vec{k}_1+\ldots+\alpha_M\vec{k}_M)\vec{r}\}. \tag{B2}$$

This leads to the following set of equations:

$$i\hbar\frac{d}{dt}\langle B_m\rangle^{(\alpha_1,\ldots,\alpha_M)}=\sum_n F_{mn}\langle B_n\rangle^{(\alpha_1,\ldots,\alpha_M)}-\sum_{j=1}^{M}E_m^{(j)}(t)\delta_{1\alpha_j}\prod_{j'\neq j}\delta_{0\alpha_{j'}}+\sum_{\alpha_1',\ldots,\alpha_M'=-\infty}^{\infty}\Bigg\{\Delta_m\langle B_m^\dagger\rangle^{(\alpha_1-\alpha_1',\ldots,\alpha_M-\alpha_M')}\times\langle B_mB_m\rangle^{(\alpha_1',\ldots,\alpha_M')}+(\kappa_m^2-2)\Bigg[\sum_n J_{mn}\langle B_m^\dagger\rangle^{(\alpha_1-\alpha_1',\ldots,\alpha_M-\alpha_M')}\langle B_nB_m\rangle^{(\alpha_1',\ldots,\alpha_M')}-\sum_{j=1}^{M}E_m^{(j)}(t)\langle B_m^\dagger\rangle^{(\alpha_1-\alpha_1',\ldots,\alpha_j-\alpha_{j'}-1,\ldots,\alpha_M-\alpha_{M'})}\langle B_m\rangle^{(\alpha_1',\ldots,\alpha_M')}\Bigg]\Bigg\} \tag{B3}$$

and

$$i\hbar\frac{d}{dt}\langle B_mB_n\rangle^{(\alpha_1,\ldots,\alpha_M)}=(1-\delta_{mn})\Bigg\{\sum_l\left[F_{ml}\langle B_lB_n\rangle^{(\alpha_1,\ldots,\alpha_M)}+F_{nl}\langle B_mB_l\rangle^{(\alpha_1,\ldots,\alpha_M)}\right]-\sum_{j=1}^{M}\left[E_n^{(j)}(t)\times\langle B_m\rangle^{(\alpha_1,\ldots,\alpha_j-1,\ldots,\alpha_M)}+E_m^{(j)}(t)\langle B_n\rangle^{(\alpha_1,\ldots,\alpha_j-1,\ldots,\alpha_M)}\right]\Bigg\}+\delta_{mn}\Bigg\{(2\hbar\Omega_m+\Delta_m-i\hbar\Gamma_m^{(2)})\times\langle B_mB_m\rangle^{(\alpha_1,\ldots,\alpha_M)}-\kappa_m^2\Bigg[\sum_{j=1}^{M}E_m^{(j)}(t)\langle B_m\rangle^{(\alpha_1,\ldots,\alpha_j-1,\ldots,\alpha_M)}+\sum_l J_{ml}\langle B_lB_m\rangle^{(\alpha_1,\ldots,\alpha_M)}\Bigg]\Bigg\}. \tag{B4}$$

(Note that $\langle B_n^\dagger\rangle^{(\alpha_1,\ldots,\alpha_M)}=[\langle B_n\rangle^{(-\alpha_1,\ldots,-\alpha_M)}]^*$.)

APPENDIX C: EXCITON SCATTERING MATRIX FOR A DIMER

In the following we give the scattering matrix, $\overline{\Gamma}(\omega)$, for a dimer using the solution of the one-exciton eigenvalue problem defined through Eqs. (4.1) and (4.2). Making use of Eq. (3.20) we have (the inverse lifetimes of the one-exciton states are assumed to be all equal to Γ which is taken as a small parameter)

$$\overline{\Gamma}_{mn}(\omega)=\frac{1}{D(\omega)}\{\delta_{mn}[\delta_{m1}\kappa_2^2d_1(\omega)+\delta_{m2}\kappa_1^2d_2(\omega)]-d_1(\omega)d_2(\omega)[P_{mn}^{++}(\omega)+P_{mn}^{--}(\omega)+2P_{mn}^{+-}(\omega)]\}. \tag{C1}$$

Here we defined $d_n(\omega)=\tilde{g}_n\kappa_n^2-q_n\hbar\omega$, and the matrix

$$P^{\alpha\beta}(\omega)=\frac{1}{\hbar(\omega-\omega_\alpha-\omega_{\beta+2i\Gamma})}\begin{pmatrix}\cos^2\Theta_\alpha\cos^2\Theta_\beta & -\sin\Theta_\alpha\sin\Theta_\beta\cos\Theta_\alpha\cos\Theta_\beta\\ -\sin\Theta_\alpha\sin\Theta_\beta\cos\Theta_\alpha\cos\Theta_\beta & \sin^2\Theta_\alpha\sin^2\Theta_\beta\end{pmatrix}. \tag{C2}$$

We have introduced

$$D(\omega)=\kappa_1^2\kappa_2^2-f_r^{++++}(\omega)-f_r^{----}(\omega)-2f_r^{+--+}(\omega)+d_1(\omega)d_2(\omega)[f^{++--}(\omega)+f^{++++}(\omega)+2f^{----}(\omega)], \tag{C3}$$

with the abbreviations

Downloaded¬08¬Mar¬2001¬to¬128.151.176.185.¬Redistribution¬subject¬to¬AIP¬copyright,¬see¬http://ojps.aip.org/jcpo/jcpcpyrts.html

$$f_r^{\alpha_1\alpha_2\alpha_3\alpha_4}(\omega)=\frac{\kappa_2^2 d_1(\omega)\sin^2\Theta_{\alpha_1}\sin^2\Theta_{\alpha_2}+\kappa_1^2 d_2(\omega)\cos^2\Theta_{\alpha_3}\cos^2\Theta_{\alpha_4}}{\hbar(\omega-\omega_{\alpha_1}-\omega_{\alpha_2}+2i\Gamma)} \tag{C4}$$

and

$$f^{\alpha_1\alpha_2\alpha_3\alpha_4}(\omega)=\frac{1}{\hbar^2(\omega-\omega_{\alpha_1}-\omega_{\alpha_2}+2i\Gamma)(\omega-\omega_{\alpha_3}-\omega_{\alpha_4}+2i\Gamma)}[\sin^2\Theta_{\alpha_1}\sin^2\Theta_{\alpha_2}\cos^2\Theta_{\alpha_3}\cos^2\Theta_{\alpha_4}$$
$$+\cos^2\Theta_{\alpha_1}\cos^2\Theta_{\alpha_2}\sin^2\Theta_{\alpha_3}\sin^2\Theta_{\alpha_4}-2\sin^2\Theta_{\alpha_1}\cos^2\Theta_{\alpha_2}\sin\Theta_{\alpha_3}\cos\Theta_{\alpha_3}\sin\Theta_{\alpha_4}\cos\Theta_{\alpha_4}]. \tag{C5}$$

The expression, Eq. (C1), was used in the calculations presented in Figs. 3–8.

[1] R. van Grondelle, J. P. Dekker, T. Gillbro, and V. Sundström, Biochim Biophys. Acta **1187**, 1 (1994); V. Sundström and R. van Grondelle, in *Anoxygenic Photosynthetic Bacteria*, edited by R. E. Blankenship, M. T. Madiga, and C. E. Baner (Kluwer Academic, Dordrecht, 1995), p. 349

[2] W. Kühlbrandt, D. N. Wang, and Y. Fujiyoshi, Nature **367**, 614 (1994).

[3] G. McDermott, S. M. Prince, A. A. Freer, A. M. Hawthornthwaite-Lawless, M. Z. Papiz, R. J. Cogdell, and N. W. Isaacs, Nature **374**, 517 (1995).

[4] S. Karrasch, P. A. Bullough, and R. Gosh, EMBO J. **14**, 631 (1995).

[5] K. Sauer, R. J. Cogdell, S. M. Prince, A. A. Freer, N. W. Isaacs, and H. Scheer, Photochem. Photobiol. **64**, 564 (1996).

[6] G. J. S. Fowler, R. W. Visschers, G. G. Grief, R. van Grondelle, and C. N. Hunter, Nature **355**, 848 (1992).

[7] S. Hess, E. Åkesson, R. J. Cogdell, T. Pullerits, and V. Sundström, Biophys. J. **69**, 2211 (1995).

[8] T. Joo, Y. Jia, J.-Y. Yu, D. M. Jonas, and G. R. Fleming, J. Phys. Chem. **100**, 2399 (1996).

[9] S. Hess, K. J. Visschers, T. Pullerits, V. Sundström, G. J. S. Fowler, and C. N. Hunter, Biochemistry **33**, 8300 (1994).

[10] L. O. Pålsson, M. D. Spangfort, V. G. Gulbinas, and T. Gillbro, FEBS Lett. **339**, 134 (1994).

[11] T. Bittner, K.-D. Irrgang, G. Renger, and M. R. Wasielewski, J. Phys. Chem. **98**, 11821 (1994); T. Bittner, G. P. Wiederrecht, K.-D. Irrgang, G. Renger, and M. R. Wasielewski, Chem. Phys. **98**, 311 (1995).

[12] D. D. Eads, E. W. Castner, R. S. Alberte, L. Mets, and G. R. Fleming, J. Phys. Chem. **93**, 8271 (1989).

[13] M. Du, X. Xie, L. Mets, and G. R. Fleming, J. Phys. Chem. **98**, 4736 (1994).

[14] H. M. Visser, F. J. Kleima, I. H. M. van Stokkum, R. van Grondelle, and H. van Amerongen, Chem. Phys. (in press).

[15] S. Mukamel, in *Molecular Nonlinear Optics*, edited by J. Zyss (Academic, New York, 1994); p. 1; F. C. Spano and S. Mukamel, Phys. Rev. Lett. **66**, 1197 (1991); O. Dubovsky and S. Mukamel, J. Chem. Phys. **95**, 7828 (1991).

[16] S. Hess, M . Chachisvilis, T. Pullerits, M. R. Jones, G. J. C. Fowler, C. N. Hunter, and V. Sundström, in *Femtochemistry—The Lausanne Conference*, edited by M. Chergui (World Scientific, Singapore, 1996), p. 379.

[17] S. L. S. Kwa, H. van Amerongen, S. Lin, J. P. Dekker, R. van Grondelle, and W. S. Struve, Biochim. Biophys. Acta **1102**, 202 (1992).

[18] J. Knoester and F. C. Spano, Phys. Rev. Lett. **74**, 2780 (1995).

[19] S. Mukamel, *Principles of Nonlinear Optical Spectroscopy* (Oxford, New York, 1995).

[20] Note that we are not implying here that S_1 is the first excited singlet state, etc. This is merely a generic notation for the excited states.

[21] A. S. Davydov, *Theory of Molecular Excitons* (Plenum, New York, 1971); V. M. Agranovich and M. D. Galanin, ''Electronic excitation energy transfer in condensed matter,'' in Modern Problems in Condensed Sciences, edited by V. M. Agranovich and A. A. Maradudin (North-Holland, Amsterdam, 1982).

[22] V. Chernyak, N. Wang, and S. Mukamel, Phys. Rep. **263**, 213 (1995).

[23] J. A. Leegwater and S. Mukamel, Phys. Rev. A **46**, 452 (1992).

[24] Note that in principle one has to solve the complex eigenvalue problem where $\Omega_n \rightarrow \tilde{\Omega}_n$ in Eq. (3.17). In photosynthetic antennae, however, $\gamma_n^{(1)}$ is very small so that there is numerically no difference whether we calculate the single-exciton Green's function from Eqs. (3.18) and (3.19) or using Eq. (3.10).

[25] Since only the largest interaction energies have been reported in Ref. 5 our excitonic energies and the oscillator strengths for the one-exciton transitions slightly deviate from those obtained in Ref. 5.

[26] S. Krawzcyk, Z. Krupa, and W. Maksymiec, Biochem. Biophys. Acta **1143**, 273 (1993).

[27] R. M. Pearlstein, in *Chlorophylls*, edited by H. Scheer (CRC Press, Boca Raton, 1991), p. 1047; X. Y. Lu and R. M. Pearlstein, Photochem. Photobiol. **57**, 86 (1993).

[28] T. Renger, ''Theoretical investigation of the energy transfer in the light-harvesting complex of Photosystem II in higher plants,'' Diploma thesis, Humboldt University, Berlin, 1995.

[29] T. Renger, J. Voigt, V. May, and O. Kühn, in Ref. 16, p. 401.

[30] H. van Amerongen, S. L. S. Kwa, B. M. Bolhuis, and R. van Grondelle, Biophys. J. **67**, 837 (1994).

[31] D. Gülen, R. van Grondelle, and H. van Amerongen, *Photosynthesis: from Light to Biosphere*, edited by P. Mathis (Kluwer Academic, Dordrecht, 1995), Vol. I, p. 335.

[32] J. F. Shepanski and R. W. Anderson, Chem. Phys. Lett. **78**, 165 (1981).

[33] M. Chachisvilis, T. Pullerits, M. R. Jones, C. N. Hunter, and V. Sundström, Chem. Phys. Lett. **224**, 345 (1994).

[34] M. H. Vos, F. Rappaport, J. C. Lambry, J. Breton, and J. L. Martin, Nature **363**, 320 (1993).

[35] O. Kühn, T. Renger, and V. May, Chem. Phys. **204**, 99 (1996).

[36] V. Chernyak and S. Mukamel, J. Opt. Soc. Am. B **13**, 1302 (1996).

[37] V. Chernyak and S. Mukamel, J. Chem. Phys. **104**, 444 (1996).

[38] T. Holstein and H. Primakoff, Phys. Rev. **58**, 1098 (1940).

[39] F. J. Dyson, Phys. Rev. **102**, 1217 (1956).

[40] V. M. Agranovich and B. S. Toshich, Sov. Phys. JETP **26**, 104 (1966).

[41] P. Ring and P. Schuck, *The Nuclear Many-Body Problem* (Springer, New York, 1980).

[42] V. Chernyak, Phys. Lett. A **163**, 117 (1992).

[43] V. Chernyak and S. Mukamel, Phys. Rev. A **52**, 3601 (1995).

[44] M. Lindberg, R. Binder, and S. Koch, Phys. Rev. A **45**, 1865 (1992).

Downloaded¬08¬Mar¬2001¬to¬128.151.176.185.¬Redistribution¬subject¬to¬AIP¬copyright,¬see¬http://ojps.aip.org/jcpo/jcpcpyrts.html